Algorithm development and validation for satellite-derived distributions of DOC and CDOM in the U.S. Middle Atlantic Bight

Antonio Mannino,[1] Mary E. Russ,[1,2] and Stanford B. Hooker[1]

Received 8 August 2007; revised 20 March 2008; accepted 31 March 2008; published 30 July 2008.

[1] Oceanographic cruises were conducted within the U.S. Middle Atlantic Bight (MAB) to collect field measurements to develop algorithms to retrieve surface ocean colored dissolved organic matter (CDOM) and dissolved organic carbon (DOC) from NASA's MODIS-Aqua and SeaWiFS satellite sensors and to investigate the processes that influence the distributions of CDOM and DOC. In order to develop empirical algorithms for CDOM and DOC, the CDOM absorption coefficient (a_{CDOM}) was correlated with in situ remote sensing reflectance band ratios, and DOC was then derived from a_{CDOM} through the a_{CDOM} to DOC relationships. Our validation analyses demonstrate successful retrieval of DOC and CDOM using MODIS and SeaWiFS with mean absolute percent differences from field measurements of 9.3 ± 7.3% for DOC, 19 ± 14% for $a_{CDOM}(355)$, 15.5 ± 12% for $a_{CDOM}(443)$, and 8.6 ± 4.9% for the CDOM spectral slope. To our knowledge, the algorithms presented here represent the first validated algorithms for satellite retrieval of a_{CDOM}, DOC, and CDOM spectral slope in the coastal ocean. Satellite imagery demonstrates the importance of riverine/estuarine discharge from Chesapeake Bay and Delaware Bay to the export of CDOM and DOC to the coastal ocean. Between spring and summer, photooxidation has a significant impact on CDOM distributions resulting in a pronounced decrease in a_{CDOM} between the midshelf and continental slope region of the MAB. The satellite-derived DOC products demonstrate the net ecosystem production of DOC of 12 to 34 μmol C L^{-1} between spring and summer. The a_{CDOM} algorithms presented here are applicable to other coastal regions and can also be used to retrieve DOC using region-specific a_{CDOM} to DOC relationships.

Citation: Mannino, A., M. E. Russ, and S. B. Hooker (2008), Algorithm development and validation for satellite-derived distributions of DOC and CDOM in the U.S. Middle Atlantic Bight, *J. Geophys. Res.*, *113*, C07051, doi:10.1029/2007JC004493.

1. Introduction

[2] Because of the large fluxes of carbon, high productivity, and potential for carbon sequestration, the coastal ocean represents an important component of the global carbon cycle. The coastal ocean accounts for 21% of the ocean's primary production [*Jahnke*, 2008]. Globally, rivers export an estimated 0.43 Pg organic carbon a^{-1} [*Schlünz and Schneider*, 2000; *Ludwig et al.*, 1996] and 0.4 Pg inorganic carbon a^{-1} to the ocean [*McKee*, 2003, and references therein]. Dissolved organic carbon (DOC) comprises over 80–90% of the organic carbon found in the coastal ocean [e.g., *Bates and Hansell*, 1999] and constitutes one of the largest pools of organic carbon in the biosphere [*Hedges*, 2002]. Hence satellite-based retrievals of DOC distributions and processes related to the cycling of DOC will improve our understanding of the coastal carbon cycle.

[3] As a consequence of the variability in the discharge of terrigenous organic matter, sediments, and detritus into coastal waters by rivers and estuaries and the occurrence of phytoplankton blooms, estuaries and the coastal ocean experience a high degree of variability in the composition and concentration of DOC, chromophoric dissolved organic matter (CDOM) and particulate matter [*Bricaud et al.*, 1981; *Carder et al.*, 1989; *Aiken et al.*, 1992]. This complicates the bio-optical properties of the coastal ocean due to the strong absorptive character of terrigenous CDOM, detritus, and phytoplankton and impedes accurate satellite-based measurements of other ocean color constituents such as chlorophyll a. In coastal waters, CDOM can dominate the inherent light absorption at ultraviolet and blue wavelengths (20–70% at 440 nm [*Del Vecchio and Subramaniam*, 2004]) and confound the retrieval of chlorophyll a from ocean color satellite observations due to overlapping absorbance spectra at blue wavelengths for both parameters [*Bricaud et al.*, 1981; *Nelson and Guarda*, 1995; *DeGrandpre et al.*, 1996]. However, the capability to quantify CDOM may lead to improvements in satellite retrievals of chlorophyll a and biogeochemical processes in the coastal ocean.

[4] Algorithms developed for the GeoEye/NASA Seaviewing Wide Field-of-view Sensor (SeaWiFS) [*Hoge et al.*,

[1]Hydrospheric and Biospheric Sciences Laboratory, NASA Goddard Space Flight Center, Greenbelt, Maryland, USA.
[2]Goddard Earth Sciences and Technology Center, University of Maryland, Baltimore County, Baltimore, Maryland, USA.

0148-0227/08/2007JC004493$09.00

2001; *Maritorena et al.*, 2002] and the NASA Moderate Resolution Imaging Spectroradiometer (MODIS) [*Carder et al.*, 1999] estimate the absorption coefficient of CDOM and detritus as a single parameter (a_{CDM}), because CDOM and detritus have similar spectral responses in the visible spectrum. Several algorithms have been developed to retrieve a_{CDM} from remote sensing of the ocean [*Carder et al.*, 1999; *Lee et al.*, 2002; *Siegel et al.*, 2002, 2005], and in the MAB specifically [*Hoge et al.*, 2001; *Magnuson et al.*, 2004]. These methods use semianalytical models to simultaneously derive multiple parameters including a_{CDM}, chlorophyll a, and the particulate backscatter coefficient. The semianalytical models require positive and accurate water-leaving radiances to retrieve the suite of absorption and backscatter products. However, atmospheric correction models applied to ocean color sensors tend to overcorrect for aerosols, particularly in coastal waters, and lead to underestimation of water-leaving radiances including negative values for the blue bands, 412 and 443 nm [*Siegel et al.*, 2000; *Bailey et al.*, 2003], which can result in poor retrievals for all algorithms that utilize the 412 and 443 nm satellite bands. Application of region-specific aerosol models and utilization of the recently implemented short-wave infrared wavelength bands on the MODIS sensor for improved atmospheric correction in turbid waters [*Wang and Shi*, 2005] should improve retrievals of the blue bands and permit the inclusion of these bands in satellite algorithms to retrieve a_{CDOM}. Furthermore, the parameterization of the semianalytical models includes only a single spectral slope for CDM [*Maritorena et al.*, 2002; *Magnuson et al.*, 2004], which is not appropriate for coastal waters where the CDOM spectral slope can vary spatially (nearshore to offshore) and seasonally [*Blough and Del Vecchio*, 2002].

[5] Satellite products are also derived through empirical methods, for example, relating the CDOM absorption coefficient (a_{CDOM}) to remote sensing reflectance (Rrs) band ratios of various ocean color bands. In fact, the operational chlorophyll a products distributed by NASA are derived from empirical models [*O'Reilly et al.*, 1998]. *D'Sa and Miller* [2003] found strong relationships between $a_{CDOM}(412)$ and several Rrs band ratios (412 nm/510 nm, 443 nm/510 nm, and 510 nm/555 nm) in the Mississippi River plume. At the CalCOFI site in southern California, *Kahru and Mitchell* [2001] applied the SeaWiFS Rrs(443)/Rrs(510) band ratio (R443/510) to retrieve $a_{CDOM}(300)$. *Johannessen et al.* [2003] linked ultraviolet (UV) attenuation coefficients (K_d) at 323 nm, 338 nm, and 380 nm to the Rrs(412)/Rrs(555) band ratio (R412/555), and also found a strong relationship between K_d and a_{CDOM} for each of the UV bands for the coastal ocean adjacent to the Chesapeake and Delaware Bays. By deriving K_d from SeaWiFS normalized water-leaving radiances, *Johannessen et al.* [2003] retrieved a_{CDOM} to within 6–50% of in situ measurements.

[6] Although past efforts have demonstrated some success in satellite retrieval of a_{CDOM}, a systematic validation effort is needed to retrieve a_{CDOM} and DOC products within coastal ocean regions as was done globally for chlorophyll a [*Maritorena et al.*, 2002; *Bailey and Werdell*, 2006] and a_{CDM} [*Siegel et al.*, 2002]. Obtaining coincident data sets of satellite and in situ observations of sufficient size for appropriate validation analysis is truly a challenge. Typically researchers evaluate the accuracy of such algorithms with field measurements and not with satellite observations, and if comparisons are made with satellite observations then the field measurements are usually not coincident with the satellite images due to cloud cover, atmospheric failure in satellite data processing, sun glint, stray light, and other satellite sensor issues. The approach presented here entails a concerted effort to obtain coincident field measurements and satellite observations from multiple cruises to acquire a sufficiently large data set permitting algorithm development from one portion of the data set and algorithm validation from the remaining data set.

[7] One global approach to estimate DOC utilizes ocean basin-specific temperature-based algorithms [*Siegel et al.*, 2002]. Although this approach has potential for the pelagic ocean, sea-surface temperature (SST) is not likely to be a good indicator of CDOM or DOC in the coastal ocean because SST in the coastal ocean is regulated primarily by solar irradiance and to a lesser extent by ocean circulation. In addition to impacts by ocean circulation, coastal ocean distributions of CDOM and DOC can be influenced by freshwater discharge and ecosystem processes, which are not necessarily linked to SST. Instead of SST, CDOM-based algorithms that incorporate remote sensing estimates of salinity would seem appropriate, since both DOC and CDOM can covary with salinity in coastal waters [e.g., *Mantoura and Woodward*, 1983; *Del Vecchio and Blough*, 2004]. At present, however, satellite-based measurements of salinity do not exist and data from planned missions such as the joint NASA-Space Agency of Argentina Aquarius mission will be too coarse (~100 km pixels) to be useful in the coastal ocean.

[8] Currently, the most practical approach to estimate DOC in coastal waters from satellite sensors requires a_{CDOM}- or a_{CDM}-based algorithms. Consequently, an empirical least squares approach is applied here to estimate DOC from a_{CDOM} by applying relationships derived from field measurements collected within the U.S. Middle Atlantic Bight (MAB). The objectives of the work described here were to develop and validate satellite algorithms for retrieval of surface ocean a_{CDOM} and DOC within the MAB to enable estimates of DOC standing stock and process measurements for DOC (net ecosystem production) and CDOM (photooxidation). The impact of freshwater discharge on coastal ocean distributions of DOC and CDOM was also examined. The benchmark applied here was to achieve a validated uncertainty to within ±35% for DOC and CDOM algorithms as ascribed to the remote sensing retrieval of surface ocean chlorophyll a for clear waters [*Bailey and Werdell*, 2006; *Hooker et al.*, 2007].

2. Methods

2.1. Study Area

[9] The focus of this study was on the continental margin of the southern MAB extending from the Delaware Bay mouth to the region south of the Chesapeake Bay mouth (Figure 1). The general circulation pattern of the MAB is an along-shore southward flow of shelf water from George's Bank (northeast of the MAB) to Cape Hatteras, North Carolina. During winter and early spring northerly winds and the along-shore current force estuarine plumes, including Chesapeake Bay [*Rennie et al.*, 1999; *Verity et al.*, 2002]

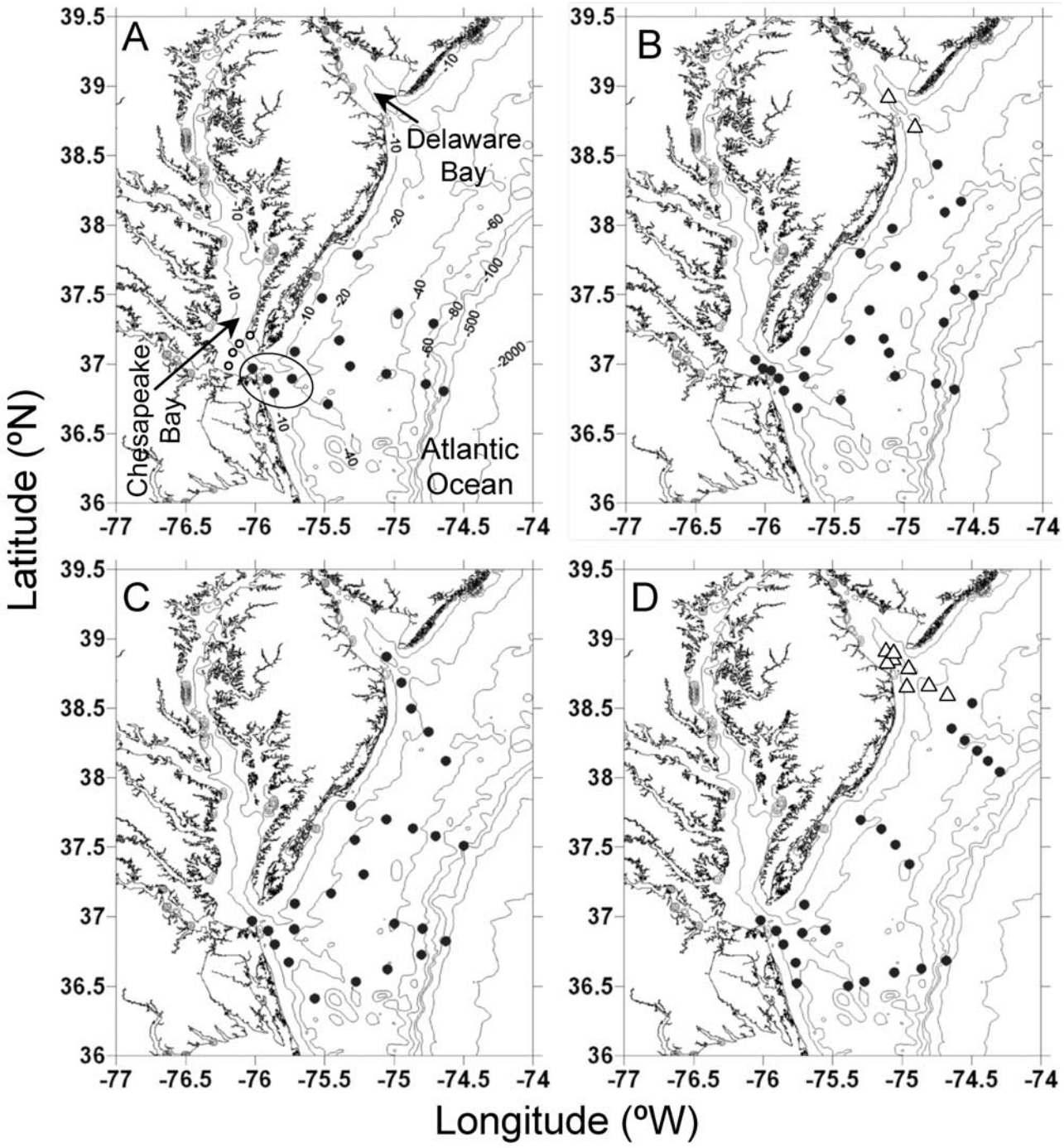

Figure 1. Map of the study area within the U.S. Middle Atlantic Bight (MAB). Station locations sampled on (A) 30 March to 1 April 2005, (B) 26–30 July 2005, (C) 9–12 May 2006, and (D) 2–6 July 2006 (solid circles and open triangles). One-day cruises were conducted in the Chesapeake Bay mouth and plume region (see ellipse in Figure 1A; 4–6 stations per cruise) on 27 May and 3 November 2005 and on 6 September and 28 November 2006. Additional samples were collected along a transect across the Chesapeake Bay mouth (open circles in Figure 1A). Isobaths shown in each panel with corresponding labels shown only in Figure 1A.

and Delaware Bay [*Sanders and Garvine*, 2001] plumes to flow southward along the coast. As winds reverse later in spring the southerly along-shore flow weakens, and the Chesapeake Bay plume broadens and flows offshore, primarily to the south and east. The surface heat flux then strengthens the water column stratification [*Verity et al.*, 2002], and saline waters from the South Atlantic Bight and the Gulf Stream flow into the southern MAB. A significant portion of shelf water from the MAB is advected offshore by the Gulf Stream from the region between Cape Hatteras

and Chesapeake Bay [*Churchill and Berger*, 1998; *Verity et al.*, 2002], which suggests that this region is an important site for carbon export to the open ocean. The drainage basin of Chesapeake Bay discharges more freshwater than any other river along the U.S. Atlantic coast, contributing about half the freshwater that flows into the MAB [*Schubel and Pritchard*, 1986]. Freshwater flowing into Delaware Bay contributes ~15–20% of the freshwater discharge entering the MAB [*Lebo and Sharp*, 1993].

2.2. Field Sampling

[10] Multiple research cruises were conducted in the southern MAB (Figure 1) from March 2005 to November 2006 (30 March to 1 April, 27 May, 26–30 July, and 3 November 2005; 9–12 May, 2–6 July, 6 September, and 28 November 2006) to collect biogeochemical (phytoplankton pigments and DOC) and apparent (AOP; water-leaving radiances) and inherent optical properties (CDOM absorption). Additional field opportunities included a series of hydrography cruises, sponsored by Old Dominion University, within the lower Chesapeake Bay between July 2004 and September 2005 (5 July, 1 September, 15 October, and 15 November 2004, 10 January, 26 May, 21 June, 19 August, and 23 September 2005; Figure 1A). Seawater samples were collected with Niskin-type bottles at multiple depths per station. The entire contents of the Niskin bottles were dispensed into carboys, which were shaken to ensure homogeneous subsampling. Additional seawater samples were collected via peristaltic pumping from ~1 m depth to obtain coincident samples with the in-water radiometer profiles.

2.3. Sample Processing, Storage, and Analysis

[11] Seawater samples for analysis of DOC and CDOM absorbance spectra were filtered under a gentle vacuum (<5 in Hg) through precombusted (6 h at 450°C) Whatman GF/F glass fiber filters and collected directly into precleaned and precombusted sample glass bottles and vials. Duplicate samples for DOC analysis were collected and stored frozen (−20°C). DOC was measured in triplicate (three of seven injections of 120 μL to maintain a standard deviation <2%) by high temperature combustion oxidation using a Shimadzu TOC-V instrument [*Benner and Strom*, 1993; *Sharp et al.*, 2002]. The deep seawater consensus reference material (CRM; Hansell Laboratory, Rosenstiel School of Marine and Atmospheric Science, University of Miami) was used daily, typically two to three sets of injections distributed throughout the day, to verify the accuracy of DOC measurements and maintain an analytical error to within ±5%. The deep seawater CRM measurements for batch 4 2004 (44.1 ± 1.7 μmol C L^{-1}; n = 50) and batch 5 2005 (45.7 ± 0.5 μmol C L^{-1}; n = 33) analyzed with these MAB samples were within reported consensus values (44–45 μmol C L^{-1} and 45–46 μmol C L^{-1}, respectively). Standard curves of the carbon standard (potassium hydrogen phthalate) ranging in concentration from 42 to 333 μmol C L^{-1} were conducted prior to sample analysis each time the catalyst was replaced. Furthermore, standards were interspersed between every 6 to 9 samples for each sample batch to verify the consistency of the standard with respect to the standard curve throughout each sample batch analyzed. The instrument carbon blank was determined from the area counts of the numerous Milli-Q ultraviolet oxidized ultrapure water injections and was subtracted from each sample analyzed.

[12] Samples for determination of CDOM spectral absorption coefficients were stored under refrigeration (4° to 8°C). In the laboratory, CDOM samples were warmed to room temperature and filtered through 0.2 μm Whatman Nuclepore (polycarbonate) filters or Gelman Supor (polyethersulfone) filters prior to analysis. Absorbance spectra of CDOM were measured using a double-beam Cary 100 Bio Ultraviolet-Visible scanning spectrophotometer and Suprasil quartz 100 mm path length cells with ultraviolet (UV) oxidized Milli-Q water as the blank and reference [*Mitchell et al.*, 2003]. Instrument scan settings were as follows: 250–800 nm wavelength scan range, 1 nm data interval, 100 nm min^{-1} scan rate, and 4 nm slit width. The instrument noise for reference baselines of air-to-air and ultrapure water spectral scans was within ±0.0005 absorbance units. Spectral absorption coefficients are determined after subtracting the raw absorption measurements with field filtration blanks of UV-oxidized Milli-Q and a null point value [*Mitchell et al.*, 2000, 2003]. For the work presented here, however, the absorbance spectra of filtration blanks and null point values were within the level of instrument noise; thus, additional corrections were not necessary. The absorption coefficients were calculated from the following expression:

$$a_{CDOM}(\lambda) = 2.303A(\lambda)/L \quad (1)$$

where $A(\lambda)$ is the absorbance of filtered seawater at a specific wavelength measured across path length L in meters. Instrument performance tests (wavelength accuracy and reproducibility, photometric noise, and baseline flatness) were conducted each day prior to analysis. Furthermore, National Institute of Standards and Technology (NIST)-traceable calibration standards (Holmium oxide filter for wavelength accuracy and Spectronics standards, Thermo Electron Corporation, to evaluate stray light, wavelength accuracy, and photometric performance) were also used to verify instrument performance. The uncertainty associated with CDOM spectral absorption coefficients at an instrument noise level <0.0046 m^{-1} was on the order of 0.023 to 0.039 m^{-1} and based on the summation of the instrument manufacturer's guaranteed specifications for photometric accuracy, stability and noise. Repeat scans of seawater subsamples, replicate subsamples, and Niskin versus persistaltic pump samples yielded a coefficient of variation of typically <±3%. The CDOM spectral slope coefficient (S) was determined by fitting a single-exponential nonlinear curve to each a_{CDOM} data set (300–700 nm):

$$a(\lambda) = a(\lambda_o)e^{-S(\lambda-\lambda_o)} \quad (2)$$

where $a(\lambda)$ and $a(\lambda_o)$ represent the absorption coefficients at wavelength λ and reference wavelength λ_o. The CDOM spectral slopes derived from equation (2) are insensitive to a_{CDOM} from higher wavelengths; i.e., equation (2) affords greater weight to a_{CDOM} values in the ultraviolet and blue spectral regions where signal-to-noise is highest.

[13] Samples for pigment analysis were collected on 25 mm GF/F filters under a gentle vacuum (<5 in Hg). Pigment samples were preserved in liquid nitrogen in the field

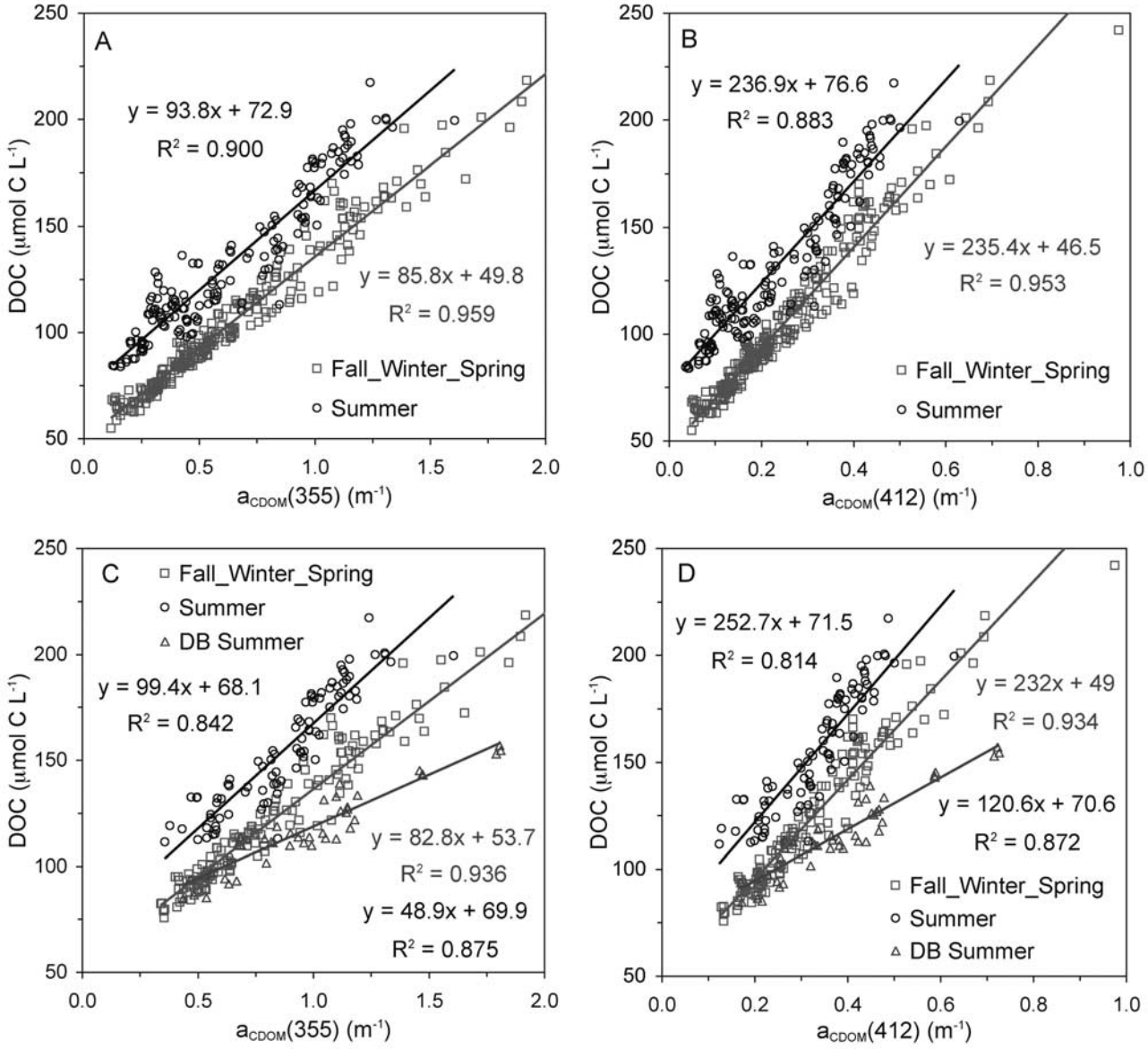

Figure 2. Seasonal relationships of dissolved organic carbon (DOC) and (A) $a_{CDOM}(355)$ (chromophoric dissolved organic matter absorption coefficient at 355 nm) or (B) $a_{CDOM}(412)$ within the MAB and between DOC and (C) $a_{CDOM}(355)$ or (D) $a_{CDOM}(412)$ in the Chesapeake Bay mouth and plume region for the 2004–2006 research cruises and Delaware Bay mouth and plume region for the summer 2005–2006 cruises (DB Summer). Data shown for Fall_Winter_Spring (October–May) include measurements from all depths sampled, but only the top 2 depths for the Chesapeake Bay mouth transect (depicted in Figure 1A). Summer (June–September) data only include the top 2 depths sampled (surface mixed layer) and exclude the Delaware Bay mouth and plume stations (open triangles in Figure 1).

and stored at −80°C in the laboratory. Pigments were analyzed by reverse-phase high-performance liquid chromatography (HPLC) at the NASA-selected laboratory in support of the NASA MODIS team (Horn Point Laboratory, University of Maryland Center for Environmental Science) [*Van Heukelem and Thomas*, 2001]. With this method, uncertainty for total chlorophyll a is 5–7% [*Claustre et al.*, 2004].

2.4. Apparent Optical Properties

[14] The BioPro, in-water profiling spectroradiometer (Biospherical Instruments, Inc.; San Diego, CA), was deployed multiples times at stations where atmospheric stability and illumination invariability over the sampling time period permitted collection of high-quality radiometric measurements. The band set for the BioPRO instrument includes the following wavelengths (each 10 nm full-width at half maximum): 320, 340, 380, 395, 412, 443, 465, 490, 510, 532, 555, 560, 625, 665, 670, 683, 710, 780, and 860 nm. Self-consistency of the data products is an important goal for the optical measurements and is defined here as the agreement between (1) modeled and measured parameters associated with attenuation scales (e.g., the euphotic

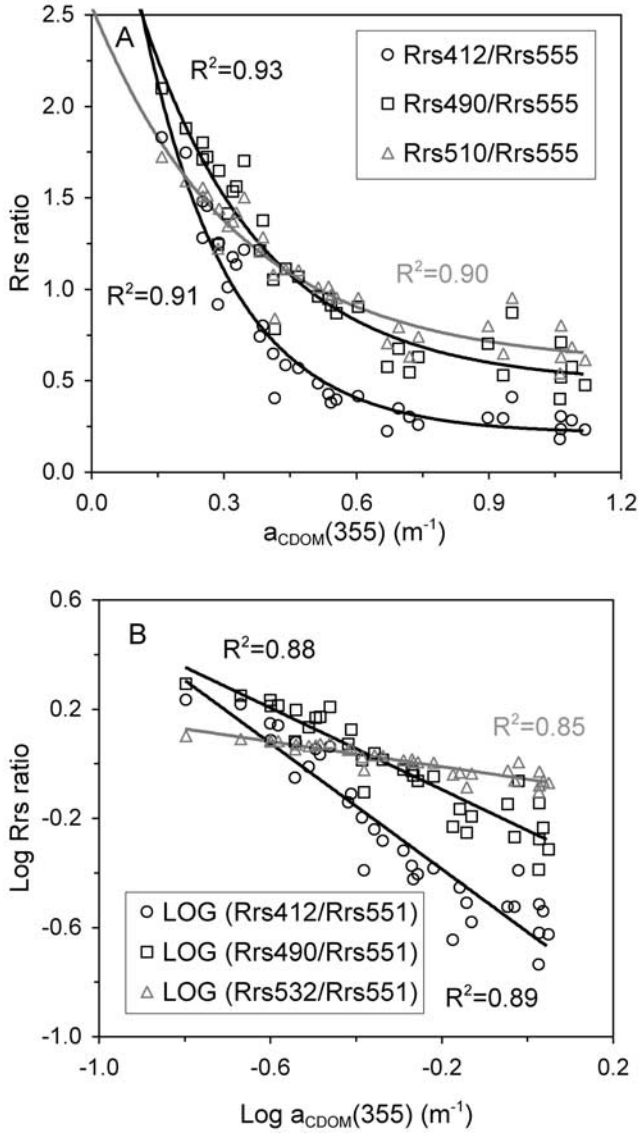

Figure 3. CDOM algorithms derived from field observations of $a_{CDOM}(355)$ and remote sensing reflectance (Rrs) band ratios include the (A) one-phase exponential decay models and (B) logarithmic models for multiple Rrs band ratios applicable to SeaWiFS and MODIS satellite sensors. The lines in each panel represent the predicted data from the nonlinear and linear regression model curve-fitting routines.

depth computed from the derived attenuation values versus the measured one percent light level); (2) derived parameters versus the known properties of seawater (e.g., the diffuse attenuation coefficients should normally exceed the values for pure water); and (3) measured and derived parameters that can be determined using more than one source or procedure (e.g., the extrapolated in-water irradiance versus the value measured by the solar reference). Some of these comparisons and the subsequent processing modifications they might trigger, might appear elementary in some cases, but for optically complex waters these procedures can be significant quality control opportunities. This high level of self-consistency is achieved from a rigorous adherence to The Ocean Optics Protocols [*Mueller*, 2003] with particular emphasis on a set of quality assurance procedures implemented during the sensor calibration, field acquisition, and data processing steps.

[15] 1. The radiometric calibration facilities are traceable to the NIST and have all been evaluated in international round robins which showed the absolute calibration uncertainties were to within 3% [*Hooker et al.*, 2002a].

[16] 2. Individual sensor characterizations (e.g., the immersion factor) have an uncertainty of less than 1% [*Hooker and Zibordi*, 2005].

[17] 3. Platform perturbations are avoided by using free-fall instruments that can be deployed far away (usually 30–50 m) from the deployment platform [*Hooker and Morel*, 2003].

[18] 4. Sensor stability is best monitored in the field with a portable source [*Hooker and Aiken*, 1998], but the short duration and limited space of small-boat operations frequently makes this impractical, so simultaneous deployments of a second similar instrument spanning the cruise time periods was used, and the intercomparison of the data products is typically to within the uncertainty in the calibrations [*Hooker et al.*, 2002b].

[19] 5. Solar irradiance data are collected with a separate sensor mounted on the deployment platform [*Hooker and Maritorena*, 2000], so small illumination variations can be removed from the profile data.

[20] 6. Two-axis tilt sensors are used to ensure only nadir radiances and planar irradiances (to within 5° of vertical) are used during data processing [*Hooker and McClain*, 2000].

[21] 7. In-water data products are derived from a near-surface extrapolation interval (a portion of the water column that starts close to the sea surface and extends downward for several or many meters as long as the water properties appear homogeneous and the log-transformed data decay linearly) and a well-established methodology [*Smith and Baker*, 1984] that has been evaluated in an international round robin [*Hooker et al.*, 2001] and shown to be capable of agreement at the 1% level.

[22] 8. Because the in-water red wavelengths decay the most rapidly, separate extrapolation intervals are used for the blue-green and red channels, and the choice in setting the deeper limit of the interval (both must have the same shallower limit) is guided by ensuring the extrapolated in-water determination of downward irradiance matches the solar reference (usually to within 2.5% and almost always to within 5%).

[23] 9. All the contemporaneous chlorophyll a data, which are needed for some of the processing options (e.g., the self-shading and bidirectional corrections), come from HPLC analysis [*Hooker et al.*, 2005].

[24] The objective is to collect AOP data with an absolute uncertainty less than 5%, so the data can be used for calibration or validation exercises with equal efficacy. One of the most useful AOP products for such inquiries is the remote sensing reflectance (Rrs), which is a primary variable for deriving satellite algorithms. In situ Rrs observations have successfully been used to quantify chlorophyll a concentrations at remote sensing wavelengths (more properly band ratios [*O'Reilly et al.*, 1998, 2000]) and the intent here is to establish ocean color algorithms to obtain satellite observations of DOC and CDOM using a similar approach.

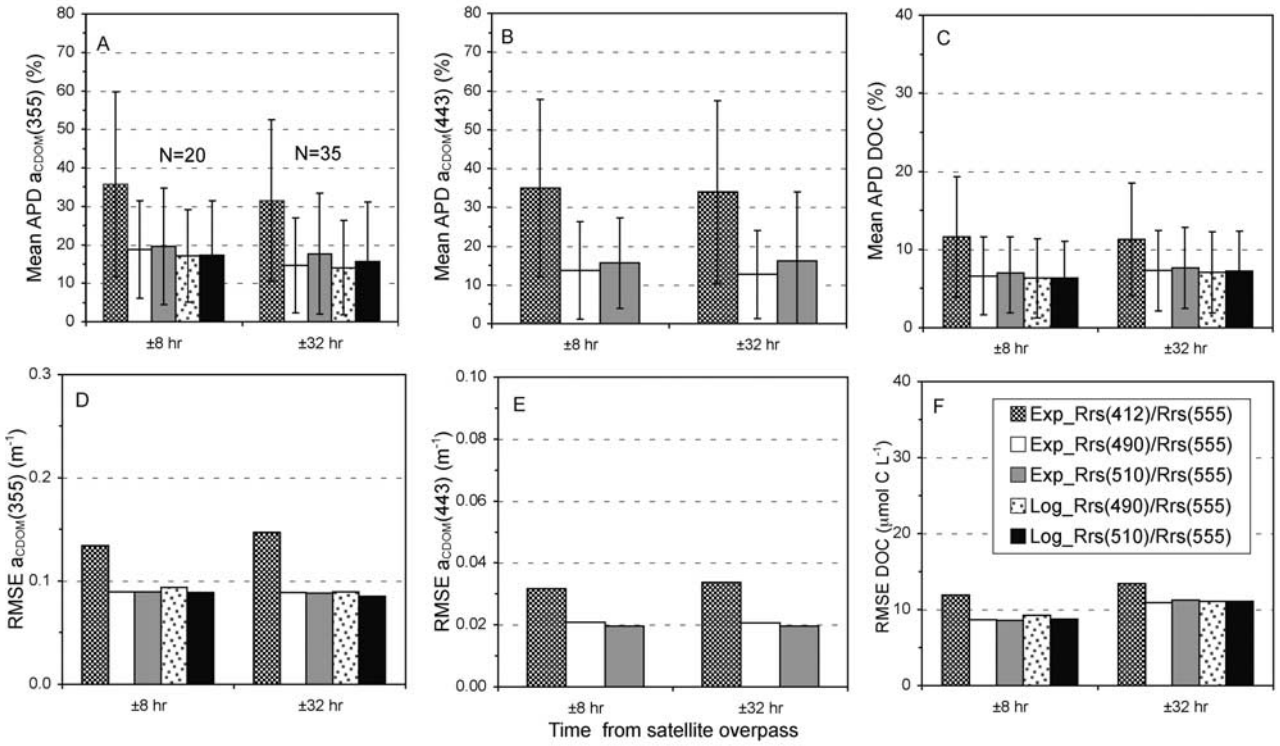

Figure 4. Validation results comparing SeaWiFS observations with field measurements for multiple algorithms within 8 h and 32 h of the satellite overpass. Figures show the mean absolute percent difference (APD) with one standard deviation for (A) $a_{CDOM}(355)$, (B) $a_{CDOM}(443)$, and (C) DOC and the root mean square error (RMSE) for (D) $a_{CDOM}(355)$, (E) $a_{CDOM}(443)$, and (F) DOC (see text for equations of APD and RMSE). Exp_Rrs(412)/Rrs(555): exponential one-phase decay algorithm for the Rrs(412 nm)/Rrs(555 nm) band ratio, Log_Rrs(490)/Rrs(555): logarithmic algorithm for the Rrs(490)/Rrs(555) band ratio. Sample sizes are the same for each panel, unless otherwise noted.

Only the AOP data collected on the 2005 research cruises (30 March to 1 April, 27 May, 26–30 July, and 3 November 2005) were applied in the work presented here.

2.5. Algorithm Development and Validation

[25] In order to develop empirical algorithms for CDOM and DOC, field measurements were collected to correlate a_{CDOM} (CDOM absorption coefficient) to Rrs band ratios and then to derive DOC from the a_{CDOM} algorithm through the a_{CDOM} to DOC relationships. Because CDOM contributes to light absorption across the visible spectrum, several band ratio solutions are possible to avoid the atmospheric correction problems associated with the 412 nm band in coastal waters (e.g., negative water-leaving radiances). The least squares approach was applied to field observations to evaluate multiple curve-fitting solutions to correlate a_{CDOM} to several Rrs band ratios including logarithmic, polynomial, power, and exponential decay functions. The curve-fitting functions, logarithmic and one-phase exponential decay, and Rrs band ratios that demonstrated the strongest linear and nonlinear regression curve-fits are presented here:

$$\mathrm{Log}[\mathrm{Rrs}(\lambda_1)/\mathrm{Rrs}(\lambda_2)] = \mathrm{slope} \bullet \log[a_{CDOM}(355)] + \mathrm{intercept} \quad (3)$$

$$\mathrm{Rrs}(\lambda_1)/\mathrm{Rrs}(\lambda_2) = b \bullet e^{-c \bullet a_{CDOM}(355)} + a \quad (4)$$

where λ_1 and λ_2 represent the various wavelengths evaluated and a, b, and c represent model coefficients. The in situ Rrs value for 551 nm was determined from a linear interpolation of the field measurements of Rrs at 532, 555, and 560 nm ($R^2 > 0.97$). The DOC and a_{CDOM} values were transformed as the inverse of DOC and natural log of $a_{CDOM}(355)$ to meet normality assumptions for model II linear regression analysis in order to derive equations relating DOC to a_{CDOM}. The CDOM spectral slope can also be derived from empirical a_{CDOM} algorithms. Relationships between a_{CDOM} and the Rrs band ratios are derived for multiple a_{CDOM} wavelengths (e.g., from 300 to 469 nm) to estimate a_{CDOM} with MODIS and SeaWiFS data at each of those wavelengths. The single exponential nonlinear curve fit described previously (equation (2)) is applied to the discrete modeled a_{CDOM} values to estimate S.

[26] The validation protocols described by *Bailey and Werdell* [2006] were applied with the exceptions that the 3 × 3 ~1 km pixel arrays (sensor native resolution) centered on the field station locations were analyzed, rather than 5 × 5 pixel arrays due to the greater spatial heterogeneity in coastal waters. In-pixel variability of field measurements may introduce errors that accentuate errors in satellite sensor retrievals [*Yuan et al.*, 2005], primarily in the bay mouth and plume regions, but is not addressed here due to a lack of in-pixel sampling. In addition, the time window between the satellite overpass and field sampling was

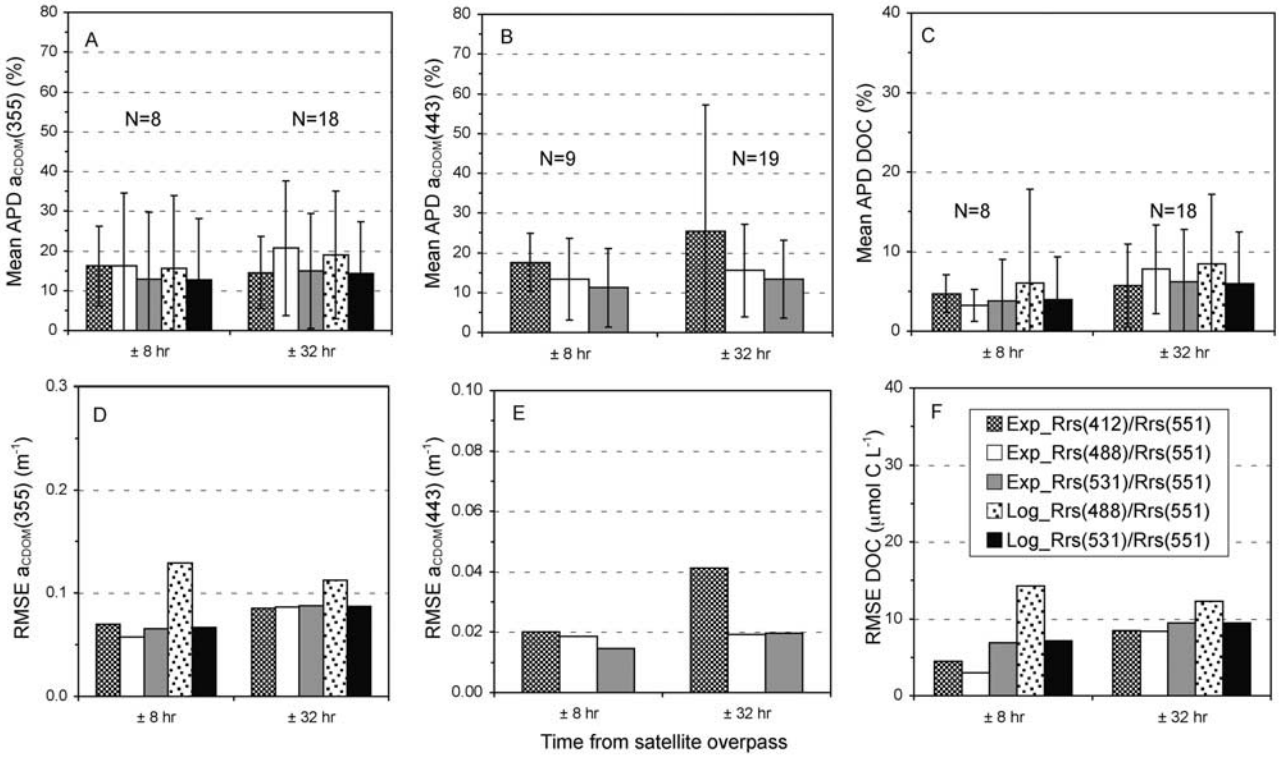

Figure 5. Validation results comparing MODIS-Aqua observations with field measurements for multiple algorithms within 8 h and 32 h of the satellite overpass. Figures show the mean APD of (A) $a_{CDOM}(355)$, (B) $a_{CDOM}(443)$, and (C) DOC and the RMSE for (D) $a_{CDOM}(355)$, (E) $a_{CDOM}(443)$, and (F) DOC. See Figure 4 for further details.

extended from 3 h to 8 and 32 h, which represent the time windows for samples collected during the day of the satellite overpass and the day before, day of, and day after the satellite overpass, respectively, to provide sufficient validation data points. An equivalent validation analysis using only the single pixel closest to the field sampling site (center pixel of 3 × 3 array) yielded poorer validation results (not shown) than the 3 × 3 pixel arrays. The averaging of the 3 × 3 pixel arrays may smooth out some of the errors associated with in-pixel and intrapixel variability as well as temporal variability. Nevertheless, the percent coefficients of variation within the 3 × 3 pixel arrays were on average 4.6–6.2% for the relevant SeaWiFS and MODIS Rrs bands (412, 443, 488, 490, 551, and 555 nm), except for the SeaWiFS 412 nm band (14%). SeaWiFS and MODIS-Aqua ocean color observations were processed using SeaDAS versions 4.9.4 and 5.0.5 (msl12 version 5.4.2) and IDL 6.1 or 6.3 from level 1A and/or 1B to level 2 data applying atmospheric corrections and masks for pixels with any of the followings flags (land, cloud or ice, high top-of-atmosphere radiance, low normalized water-leaving radiance at 555 or 551 nm, stray light, sun glint, or atmospheric correction failure) as detailed by *Bailey and Werdell* [2006]. Pixels with water-leaving radiance values <0.2 mW cm^{-2} μm^{-1} sr^{-1} were excluded (primarily the 412 nm band) to minimize the impacts of atmospheric correction that may cause negative or reduced water-leaving radiances [*Siegel et al.*, 2002]. Validation results presented here exclude all stations where in situ radiometry measurements were applied to derive the satellite sensor algorithms to ensure that the validation data set is independent from the data set used to derive the CDOM algorithms, except where otherwise noted. Multiple band-ratio algorithms were evaluated with the algorithms described here yielding similar validation results. The satellite images presented here were derived from the exponential one-phase decay relationship between a_{CDOM} and Rrs(488)/Rrs(551) (R488/551) for MODIS-Aqua and Rrs(490)/Rrs(555) (R490/555) for SeaWiFS.

[27] The evaluation of algorithm performance was based on statistical parameters comparing the satellite-derived retrievals of a_{CDOM}, DOC, and CDOM spectral slope with the field measurements, which are referred to here as validation match-ups. The statistical parameters applied include the mean and standard deviation of the absolute percent difference (APD), root mean square error (RMSE), and the R^2 and slope values from linear regression analyses of the validation match-ups for each satellite sensor [*Bailey and Werdell*, 2006; *Garcia et al.*, 2006]. In the following equations, C_{alg} and $C_{in\ situ}$ represent the parameters of interest (DOC or a_{CDOM}) for the satellite algorithm and field observations, respectively, and N refers to the sample size.

$$\text{Mean APD}(\%) = \left[\sum \left|\left(C_{alg} - C_{in\ situ}\right)\right| / C_{in\ situ}\right] * 100/N \quad (5)$$

$$\text{RMSE} = \left[1/N * \sum \left(C_{alg} - C_{in\ situ}\right)^2\right]^{1/2} \quad (6)$$

Table 1. Validated Satellite a_{CDOM} Algorithms Derived From Field Observations of $a_{CDOM}(\lambda)$ and Remote Sensing Reflectance (Rrs) Band Ratios[a]

Product	Algorithm Notation	Rrs Band Ratio	a	b	c	RMSE[b]	R^2
$a_{CDOM}(355)$	CO_a355S	490/555	0.4847	3.055	3.642	0.1496	0.908
	CO_a355M	490/551	0.4934	2.731	3.512	0.1377	0.907
$a_{CDOM}(412)$	CO_a412S	490/555	0.4443	2.599	8.327	0.1354	0.925
	CO_a412M	490/551	0.4553	2.345	8.045	0.1244	0.924
$a_{CDOM}(443)$	CO_a443S	490/555	0.4247	2.453	13.586	0.1482	0.910
	CO_a443M	490/551	0.4363	2.221	13.126	0.1355	0.910

[a]The form of the algorithm is the nonlinear one-phase exponential decay regression model: Rrs ratio = b • $e^{-c \bullet a_{CDOM}(355)}$ + a. The non-linear function was solved for a_{CDOM} yielding the following equation: $a_{CDOM}(\lambda) = \ln[(\text{Rrs ratio} - a)/b]/(-c)$. The Rrs(490 nm/551 nm) band ratio algorithms were applied to derive a_{CDOM} from MODIS-Aqua, and no adjustments were made to field-derived Rrs at 490 nm to match the 488 nm MODIS-Aqua band. The sample size was 34 for each algorithm.

[b]RMSE, Root Mean Square Error represents the standard deviation of the residuals for the Rrs band ratios from the non-linear regression analysis.

Redundant data (multiple observations from a single satellite sensor for an individual validation station) were excluded based on meeting the validation criteria for atmospheric corrections and masking due to flags [*Bailey and Werdell*, 2006] and minimum time difference between satellite overpass and field sample collection. Excluding stations where in situ radiometry measurements were applied to derive the satellite sensor algorithms reduces sample size significantly (N = 8 and 20 for MODIS-Aqua ±8 h and ±32 h validation period, respectively, rather than N = 14 and 27) and limits this MODIS-Aqua validation data set to the May 2006 sampling. Therefore results for the expanded validation data set that include stations where in situ radiometry measurements were used for algorithm development are also presented to extend the MODIS-Aqua validation into summer and fall and augment the Chesapeake Bay plume data set, which extends the upper range of DOC and a_{CDOM}. Sample size is substantially greater for SeaWiFS validation match-ups primarily due to masking of MODIS-Aqua pixels caused by flags associated with sun glint and stray light.

3. Results and Discussion

3.1. CDOM to DOC Relationships

[28] In coastal ocean waters, distributions of DOC and CDOM vary seasonally and interannually due to multiple source inputs, including in situ primary production, contributions from adjacent ocean waters, and terrigenous, anthropogenic, and estuarine-derived organic matter entering the coastal ocean from rivers and bays, and removal processes such as advection, microbial remineralization, and photooxidation. CDOM represents only a portion of the total DOC pool, and the nonchromophoric content of DOC varies seasonally and regionally due to diverse inputs and losses. The results show strong but seasonally variable relationships between a_{CDOM} and DOC for the southern MAB (Figures 2A–2B; $R^2 > 0.88$). Moreover, the seasonal relationships are consistent from year-to-year during our study period (2005–2006). For the shelf region, the a_{CDOM}-DOC slopes for the two seasonal relationships are similar (Figures 2A–2B), whereas the y-intercepts for the summer relationships are much greater than the fall-winter-spring relationships (Figures 2A–2B). Furthermore, subsets of these data from the Chesapeake Bay mouth and nearby inner-shelf demonstrate equivalent seasonal relationships (Figures 2C–2D) to the greater MAB region. In contrast, the summer a_{CDOM} to DOC relationship for the Delaware Bay mouth and nearby plume stations differs from the MAB relationship (Figure 1; Figures 2C–2D). This may be due dissimilarities in source inputs, particularly anthropogenic contributions to Delaware Bay DOM from highly absorbing petroleum hydrocarbons [*Mannino and Harvey*, 1999], black carbon [*Mannino and Harvey*, 2004], and other aromatic compounds [*Mannino and Harvey*, 2000].

[29] At least two seasonal algorithms (fall-winter-spring and summer) are required to retrieve DOC from MODIS and SeaWiFS in the MAB due to seasonal variability in the a_{CDOM} to DOC relationship caused by the accumulation of primarily nonchromophoric DOC from net ecosystem production and the concomitant loss of CDOM through sunlight-induced photooxidation between late spring to early fall [*Vodacek et al.*, 1997]. Net ecosystem production (NEP)

Table 2. DOC Algorithms Derived From Model II Linear Regression Analysis of DOC and $a_{CDOM}(355)$ Field Measurements[a]

Season	Region	Algorithm Notation	m	b	N[b]	RMSE[c]	R^2	p
Fall-Winter-Spring[d]	MAB	CO_DOC_{FWS}	0.0047465	0.0075058	277	0.000618	0.954	<0.0001
	CBP[f]	CBP_DOC_{FWS}	0.0046740	0.0073888	148	0.000517	0.938	<0.0001
Summer[e]	MAB	CO_DOC_{Su}	0.0030323	0.0061522	160	0.000684	0.874	<0.0001
	CBP[f]	CBP_DOC_{Su}	0.0034165	0.0060366	87	0.000519	0.813	<0.0001

[a]The Chesapeake Bay mouth and plume equations represent a subset of the MAB dataset. Data were transformed to meet normality assumptions of linear regression analysis. The equation takes the following form: $DOC = 1/\{\ln[a_{CDOM}(355)] \bullet (-m) + b\}$. The $a_{CDOM}(355)$ algorithms shown in Table 1 can be entered into this equation to obtain DOC directly from satellite Rrs products.

[b]N - sample size.

[c]RMSE - Root Mean Square Error refers to DOC in transformed units (1/DOC).

[d]Fall-Winter-Spring - October to May.

[e]Summer - June to September.

[f]CBP - Chesapeake Bay mouth and plume.

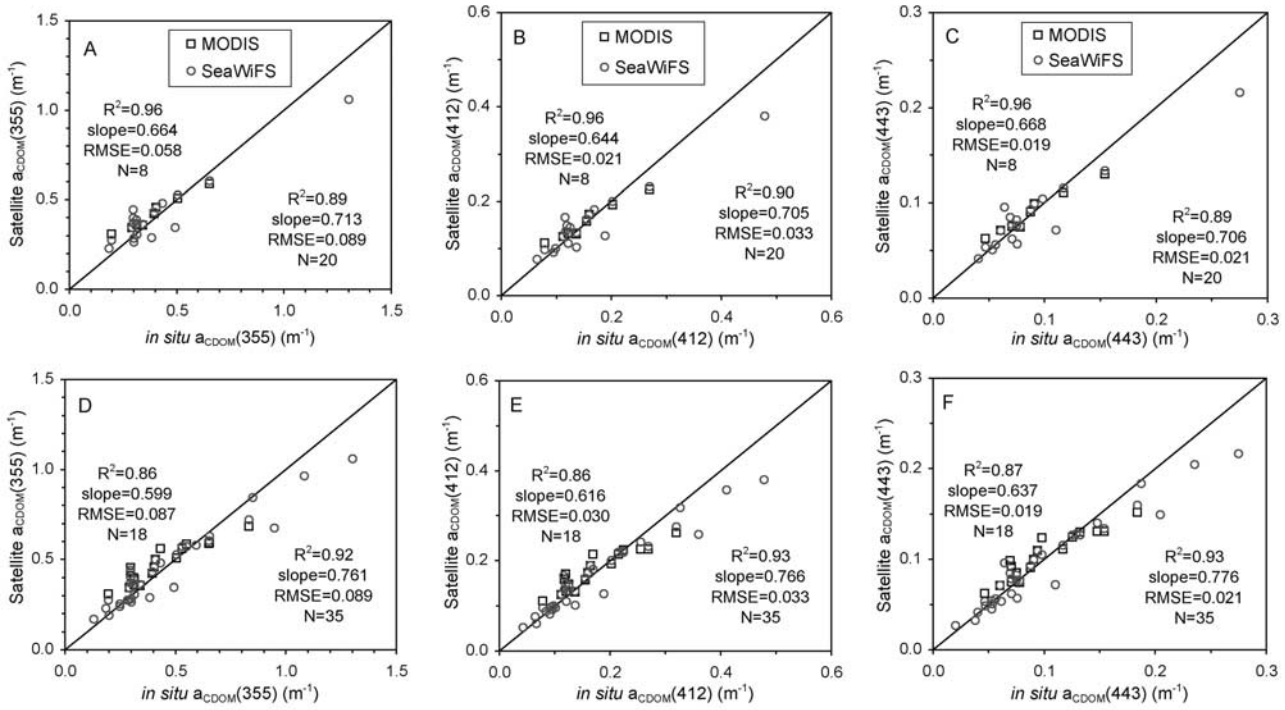

Figure 6. Validation match-ups comparing MODIS-Aqua- and SeaWiFS-derived products with field measurements for (A) $a_{CDOM}(355)$, (B) $a_{CDOM}(412)$, and (C) $a_{CDOM}(443)$ within 8 h of satellite overpass and for (D) $a_{CDOM}(355)$, (E) $a_{CDOM}(412)$, and (F) $a_{CDOM}(443)$, within 32 h of a satellite overpass. The diagonal solid line within each panel represents the one-to-one line. The statistics within the figures represent the results from the linear regression analysis of the match-up data points. The RMSE is computed as described in the text (equation (2)). The statistics above the one-to-one line refer to the MODIS-Aqua analysis, and values below the one-to-one line refer to the SeaWiFS analysis.

of DOC, which can be generally defined as the sum of phytoplankton extracellular release, lysis of phytoplankton, and zooplankton sloppy feeding and egestion minus microbial uptake, comprises approximately 20% of total primary production in the ocean [*Hansell and Carlson*, 1998; *Álvarez-Salgado et al.*, 2001]. The transitions in the seasonal DOC algorithms occur between late May and end of June and early October to early November. Smoothing algorithms for the transitional periods have been developed, but are not presented here due to a lack of validation data needed to evaluate them.

[30] Previous studies in coastal waters also show generally strong correlations between a_{CDOM} and DOC. In the southern Baltic Sea, *Ferrari et al.* [1996] observed a strong relationship between DOC and $a_{CDOM}(355)$ for April and September cruises (R = 0.9 and 0.7, respectively), and a poor correlation for an August cruise. *Del Castillo et al.* [1999] examined DOC and CDOM absorption within the Orinoco River plume in the Caribbean Sea and found a statistically significant correlation (R = 0.88) between DOC and $a_{CDOM}(300)$. Results along a transect from the Delaware Bay mouth to the Sargasso Sea showed a strong correlation between fluorescence and $a_{CDOM}(355)$ and also between fluorescence and DOC concentration [*Vodacek et al.*, 1995, 1997]. *Rochelle-Newall and Fisher* [2002] found a statistically significant relationship between $a_{CDOM}(355)$ and DOC ($P < 0.01$, $R^2 = 0.59$) within Chesapeake Bay. In a previous study of the MAB, the relationship between DOC and $a_{CDOM}(355)$ in the surface mixed layer was significant ($R^2 = 0.50$ to 0.75) but seasonally variable from summer to autumn [*Del Vecchio and Blough*, 2004], which is consistent with the results presented here. However, the equations relating DOC and $a_{CDOM}(355)$ by *Del Vecchio and Blough* [2004; e.g., July 1998: $DOC = 55.6\ a_{CDOM}(355) + 98.3$] are substantially different from the results presented here (Figure 2A). Nevertheless, the *Del Vecchio and Blough* [2004] regression slope, but not the y-intercept, from July 1998 is consistent with the 2005–2006 Delaware Bay plume summer relationship (Figure 2C; $DOC = 48.9\ a_{CDOM}(355) + 69.9$). These disparities are likely due to differences in end-member sampling, since the data from *Del Vecchio and Blough* [2004] extended from Delaware Bay to the Gulf Stream and Sargasso Sea, whereas our study emphasized the region between the Chesapeake Bay mouth and the shelf break.

3.2. CDOM and DOC Algorithm Development and Validation

[31] Several nonlinear and linear curve-fitting routines model the field observations of a_{CDOM} and Rrs band ratios rather well. The algorithms presented here include the exponential one-phase decay models (equation (4)) and the linear regression models applied to log-transformed data from the ship-based measurements of Rrs and discrete determinations of a_{CDOM} from near-surface samples (equation (3); Figure 3). The exponential decay models

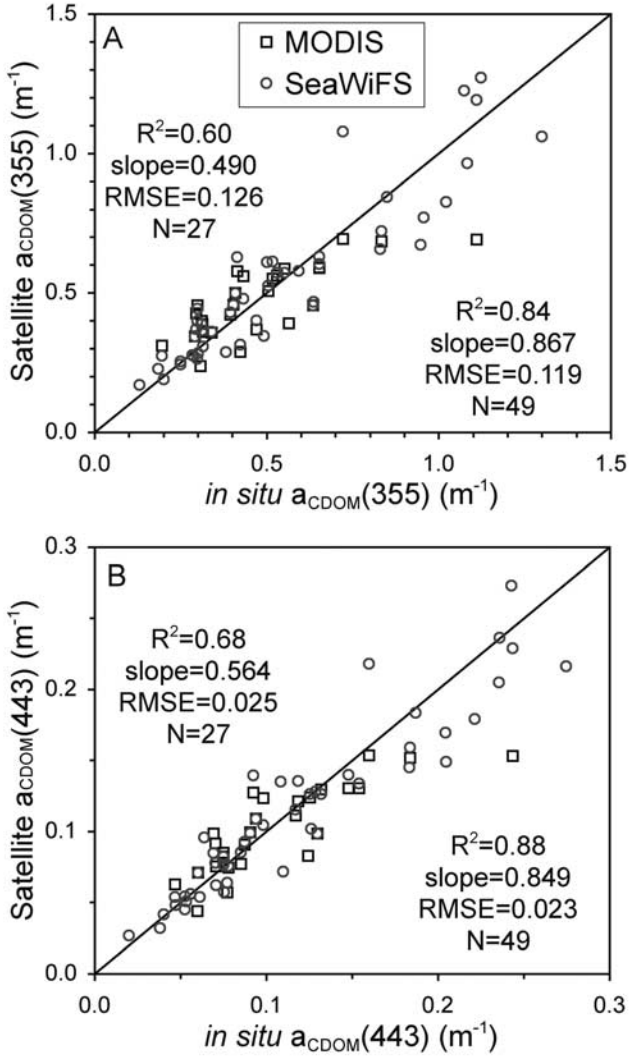

Figure 7. Match-ups of the expanded validation data set comparing MODIS-Aqua- and SeaWiFS-derived products with field measurements for (A) $a_{CDOM}(355)$ and (B) $a_{CDOM}(443)$ within 32 h of a satellite overpass. The expanded validation data set includes stations where in situ radiometry measurements were used for algorithm development. Statistics above the one-to-one line refer to MODIS-Aqua analysis, and values below the one-to-one line refer to the SeaWiFS analysis. See Figure 6 caption for additional details.

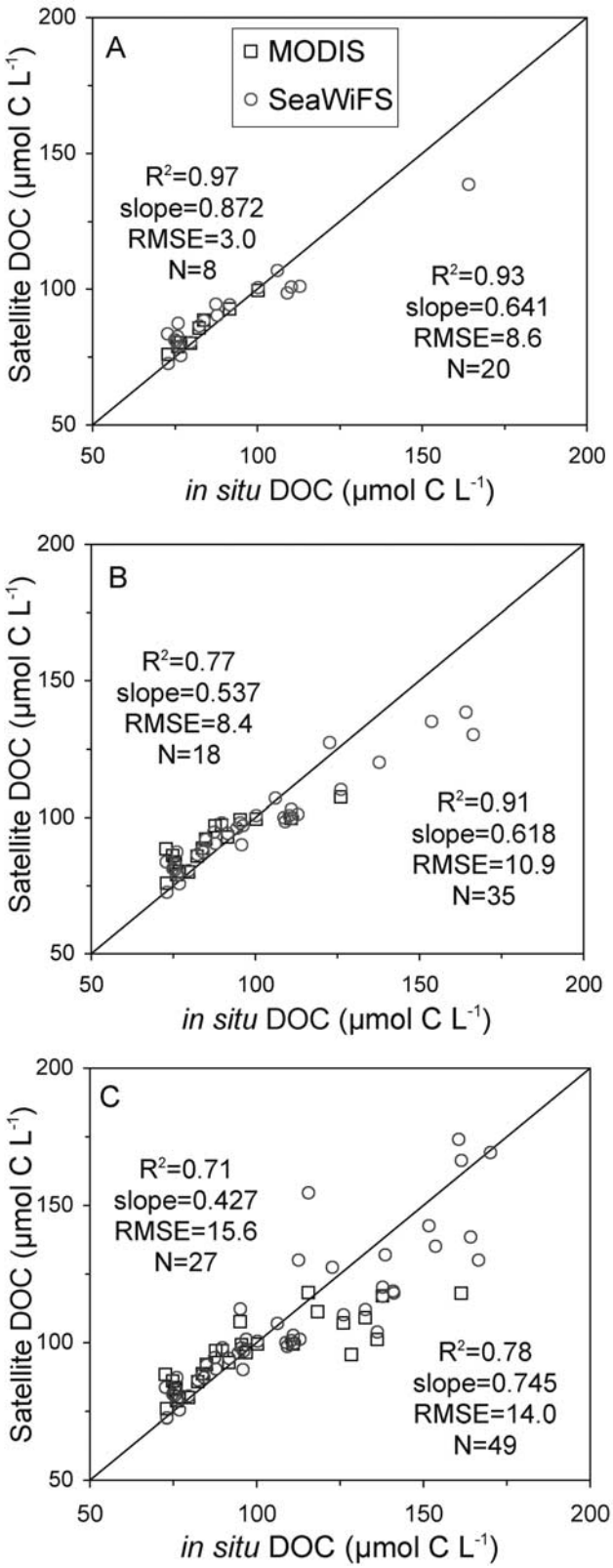

Figure 8. Validation match-ups comparing MODIS-Aqua- and SeaWiFS-derived products with field measurements of (A) DOC within 8 h of satellite overpass, (B) DOC within 32 h of satellite overpass, and (C) DOC within 32 h of satellite overpass for the expanded data set. See Figure 7 for additional details.

suggest a stronger fit for the field data (Figure 3A; R^2 of 0.90 to 0.93) than the logarithmic algorithms (Figure 3B; R^2 of 0.85 to 0.89). These field measurements suggest that several Rrs band ratios can be applied to retrieve a_{CDOM} from satellite sensors (Figure 3). Alternative algorithms can also be derived for a_{CDOM} at other wavelengths.

[32] SeaWiFS- and MODIS-Aqua-derived estimates of a_{CDOM} and DOC were compared with field observations to determine which algorithms performed best (Figures 4–5). The mean absolute percent difference (APD) and root mean square error (RMSE) for SeaWiFS (Figure 4) and MODIS-Aqua (Figure 5) a_{CDOM} (mean APD of 12.7–35.8%) and DOC (mean APD of 3.2–11.6%) products

demonstrate comparable results for most of the algorithms. Nevertheless, the algorithms based on the R412/555 band ratio performed poorly in the SeaWiFS validation compared to the other band ratios (Figure 4). The exponential one-phase decay algorithms with the R488/551 and R490/555 band ratios were selected based on the results shown (Figures 3–5) and the relative consistency in band ratios for the satellite sensors. The mean APD between the satellite sensor and field measurements are approximately 18 ± 14% for $a_{CDOM}(355)$ (mean ± 1 standard deviation), 14 ± 12% for $a_{CDOM}(443)$ and 7.4 ± 5.3% for DOC (Figures 4–5). Furthermore, expanding the validation data set to include stations where in situ radiometry measurements were used for algorithm development yields equivalent mean APD values for $a_{CDOM}(355)$ and $a_{CDOM}(443)$ (19 ± 14% and 15.5 ± 12%, respectively), but higher values for DOC (7.8 ± 8.9% and 10.1 ± 8.0% for MODIS-Aqua ±8 h and ±32 h overpass periods, respectively, and 9.3 ± 7.8% and 8.9 ± 6.9% for SeaWiFS ±8 h and ±32 h overpass periods, respectively). The equations and coefficients for the validated a_{CDOM} and DOC algorithms are described in Tables 1 and 2, respectively.

[33] The validation match-ups of satellite-derived $a_{CDOM}(355)$, $a_{CDOM}(412)$ and $a_{CDOM}(443)$ for these algorithms with the field observations demonstrate a close correspondence to the one-to-one relationship for both SeaWiFS and MODIS-Aqua (Figure 6). For $a_{CDOM}(355)$, $a_{CDOM}(412)$ and $a_{CDOM}(443)$, the SeaWiFS match-ups (R^2 = 0.89 to 0.93; slope = 0.70 to 0.78) are comparable to MODIS-Aqua (R^2 = 0.86 to 0.96; slope = 0.60 to 0.67) (Figure 6). If the validation match-up data set is expanded to include stations where in situ radiometry measurements were used for algorithm development then the match-up results improve for SeaWiFS ($a_{CDOM}(355)$: slope = 0.87 to 0.93) but deteriorate for MODIS ($a_{CDOM}(355)$: R^2 = 0.66 to 0.86; slope = 0.47 to 0.60) (Figure 7). The slope values from the one-to-one validation linear regression analyses may not represent the most informative measure of algorithm performance given the small sample size of the validation data set and the relatively narrow range of a_{CDOM} values (about one order of magnitude).

[34] Several factors can lead to discrepancies between field measurements and satellite-based observations including errors associated with field-based bio-optical algorithms (Figure 3), within pixel variability, band-to-band differences between in situ and satellite sensors (spectral bandwidth and band center), and temporal offsets between field sampling and satellite image acquisition. The expanded data set includes additional stations within the Chesapeake Bay plume region (primarily from 27 May and 3 November 2005). The additional data may accentuate discrepancies in time and space between water masses (due to tides and estuarine outflow) observed by the satellite sensor and sample collection from the ship. Furthermore, differences in Rrs between the in situ radiometry (490 nm and 555 nm bands) and the MODIS sensor (488 nm and the interpolated 551 nm bands) could be magnified because of the more optically complex waters (higher chlorophyll a, suspended particles, and CDOM) in the plume region compared to validation stations from the mid and outer-shelf. Nevertheless, the mean APD for $a_{CDOM}(355)$, $a_{CDOM}(412)$ and $a_{CDOM}(443)$ are essentially equivalent for the independent validation and expanded data sets for both sensors. Furthermore, the vertical heterogeneity in river and estuary outflow regions complicates the comparison of the satellite-derived product and the field measurement selected to represent that particular pixel in the validation match-up. Surface mixed layers were typically one to several meters in depth within the plume regions of Chesapeake Bay and Delaware Bay, and Niskin-type sampling bottles homogenized 0.5 to 1 m layer of the water column. The approach applied here entailed using measurements from only the near surface depth of the water column sampled, typically 0.5 to 2 m. For autumn and spring cruises, the DOC and a_{CDOM} values do not vary with depth from the surface to at least 100 m except within the bay mouths and nearby plume stations due to estuarine stratification.

[35] The validation match-ups demonstrate retrieval of CDOM with mean APD values for $a_{CDOM}(355)$ ranging from 14.7±12.4% for SeaWiFS to 20.6 ± 16.9% for MODIS (Figures 4–5). For $a_{CDOM}(443)$, the mean APD values range from 12.7 ± 11.3% for SeaWiFS to 15.5 ± 11.6% for MODIS (Figures 4–5). These mean APD values are quite reasonable by comparison with typical satellite retrievals of chlorophyll a globally (33.1% median percent difference [*Bailey and Werdell*, 2006]) or within continental margins such as the southwestern Atlantic Ocean (66–250% APD [*Garcia et al.*, 2006]) and retrievals of $a_{CDOM}(350)$ (6–50% [*Johannessen et al.*, 2003]) for the southern MAB. *Siegel et al.* [2002] reported an R^2 value of 0.63 for log transformed match-ups of SeaWiFS-derived and in situ $a_{CDM}(440)$ for an extensive data set representing coastal ocean and open ocean sites. Satellite retrievals of $a_{CDOM}(443)$ in the southern MAB using the SeaWiFS (CO_a443S; $a_{CDOM}(443) = \ln[(Rrs\ 490/Rrs555 - 0.4247)/2.453]/ - 13.586$) and MODIS (CO_a443M; $a_{CDOM}(443) = \ln[(Rrs\ 490/Rrs551 - 0.4363)/2.221]/ - 13.126$) coastal ocean $a_{CDOM}(443)$ algorithms presented herein (Table 1) yielded an R^2 of 0.88–0.93 for SeaWiFS and an R^2 of 0.68–0.96 for MODIS-Aqua (Figures 6–7). Direct comparisons of a_{CDOM} or a_{CDM} satellite retrievals with other previously published studies is not possible due to a lack of comparable match-up validation parameters such as percent differences and regression values or absence of a robust validation analysis due to insufficient coincident satellite observations with field data.

[36] The DOC validation match-ups show close agreement between satellite retrievals and field observations (R^2 = 0.71 to 0.97; Figure 8). Given the narrow range of DOC concentrations (72 to 162 μM DOC) and limited sample size, the slope from the one-to-one linear regression analyses (0.43 to 0.87; Figure 8) is not a useful parameter to evaluate algorithm performance. The APD for DOC match-ups also demonstrate close agreement between satellite sensor and field measurements with mean APD values ranging from 3.2 ± 2.0% to 7.8 ± 5.6% for MODIS ±8 h and ±32 h satellite overpass period, respectively, and 6.6 ± 5.0% to 7.3 ± 5.2% for SeaWiFS (Figures 4–5). The RMSE values range from 8.6 to 10.9 μM DOC for SeaWiFS and 3.0 to 8.4 μM DOC for MODIS-Aqua. Higher mean APD (10.1 ± 8.0% for MODIS-Aqua and 8.9 ± 6.9% for SeaWiFS) and RMSE values (Figure 8C) were computed for the ±32 h expanded data set, which includes additional stations from summer and fall cruises and from the Ches-

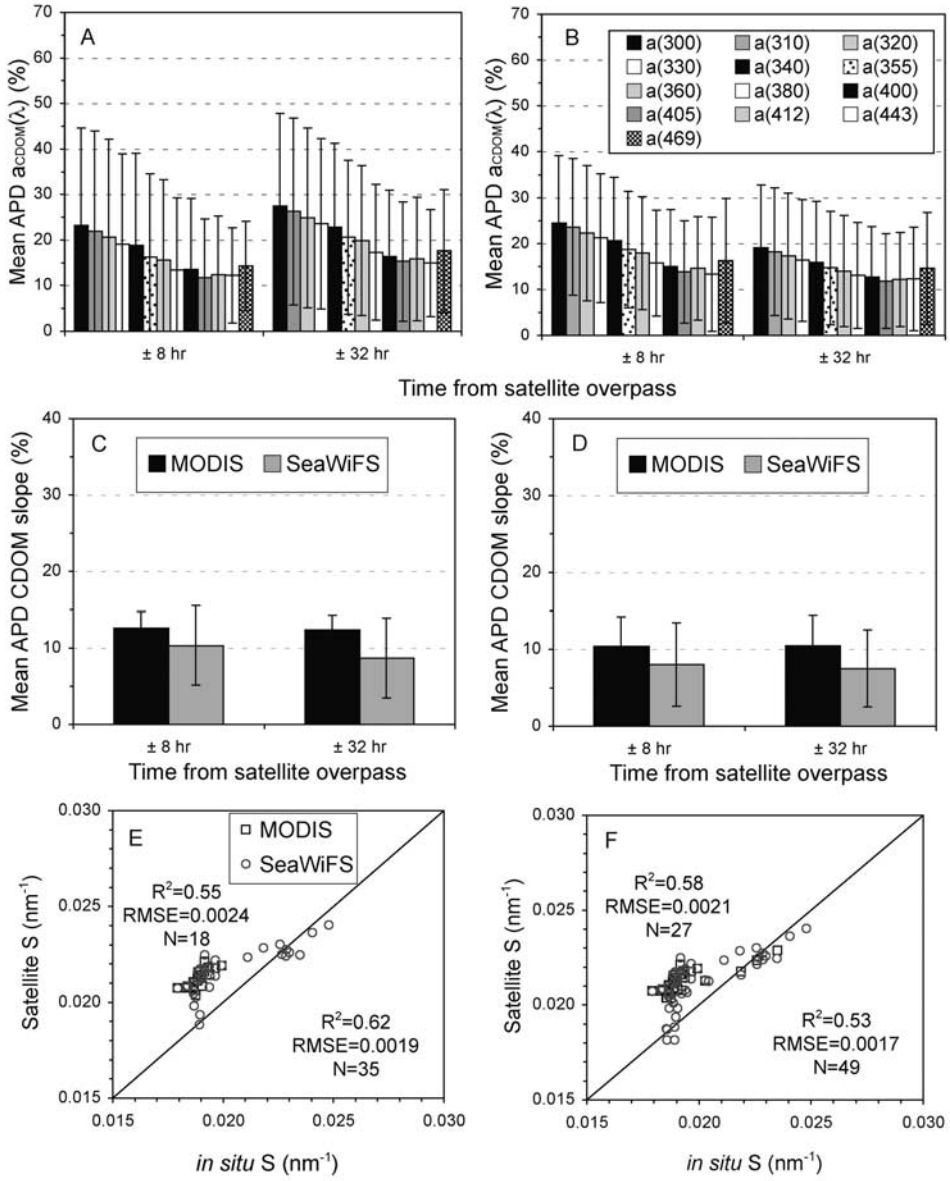

Figure 9. Validation comparisons of multiple a_{CDOM} wavelengths for (A) MODIS-Aqua and (B) SeaWiFS and the CDOM spectral slope (S) (C) mean APD, (D) mean APD for expanded validation data set, (E) one-to-one match-ups, and (F) one-to-one match-ups for the expanded validation data set.

apeake Bay plume region as described for the a_{CDOM} match-ups. This study represents the first validated algorithms for retrieval of surface ocean DOC from SeaWiFS and MODIS satellite sensors. The approach described by *Siegel et al.* [2002] to determine surface DOC using sea-surface temperatures may prove to be successful for entire ocean basins, but is not appropriate for coastal ocean waters just as CDOM- or CDM-based algorithms are not appropriate for the open ocean because of the poor and sometimes negative correlation between a_{CDOM} and DOC in the open ocean.

[37] To derive an algorithm for the CDOM spectral slope (S), coefficients from the exponential one-phase decay Rrs band ratio models (equation (4)) using the R490/555 or R488/551 band ratios were computed for multiple a_{CDOM} wavelengths (300, 310, 320, 330, 340, 355, 360, 380, 400, 405, 412, 443, and 469 nm). Equation (2) was fitted to these satellite-derived a_{CDOM} values to obtain S. The mean APD for $a_{CDOM}(\lambda)$ used to derive S range from 11.8 ± 12.9% to 27.5 ± 20.3% (Figures 9A–9B). The validation results suggest that the CDOM spectral slope can be retrieved from MODIS-Aqua and SeaWiFS to within 12.4 ± 1.9% and 8.7 ± 5.2% for the ±32 h data sets, respectively (Figures 9C–9D). The one-to-one match-ups for S indicate that the SeaWiFS and MODIS-Aqua products are biased slightly on the high side compared to field observations (Figures 9E–9F). The relatively narrow range of S observed in the MAB requires particularly accurate satellite retrievals (<10 ± 5%) to apply this product in tracking sources of terrigenous or marine CDOM and evaluating the extent of CDOM photooxidation. The validation results suggest that the CDOM spectral slope algorithms can be useful for these applications.

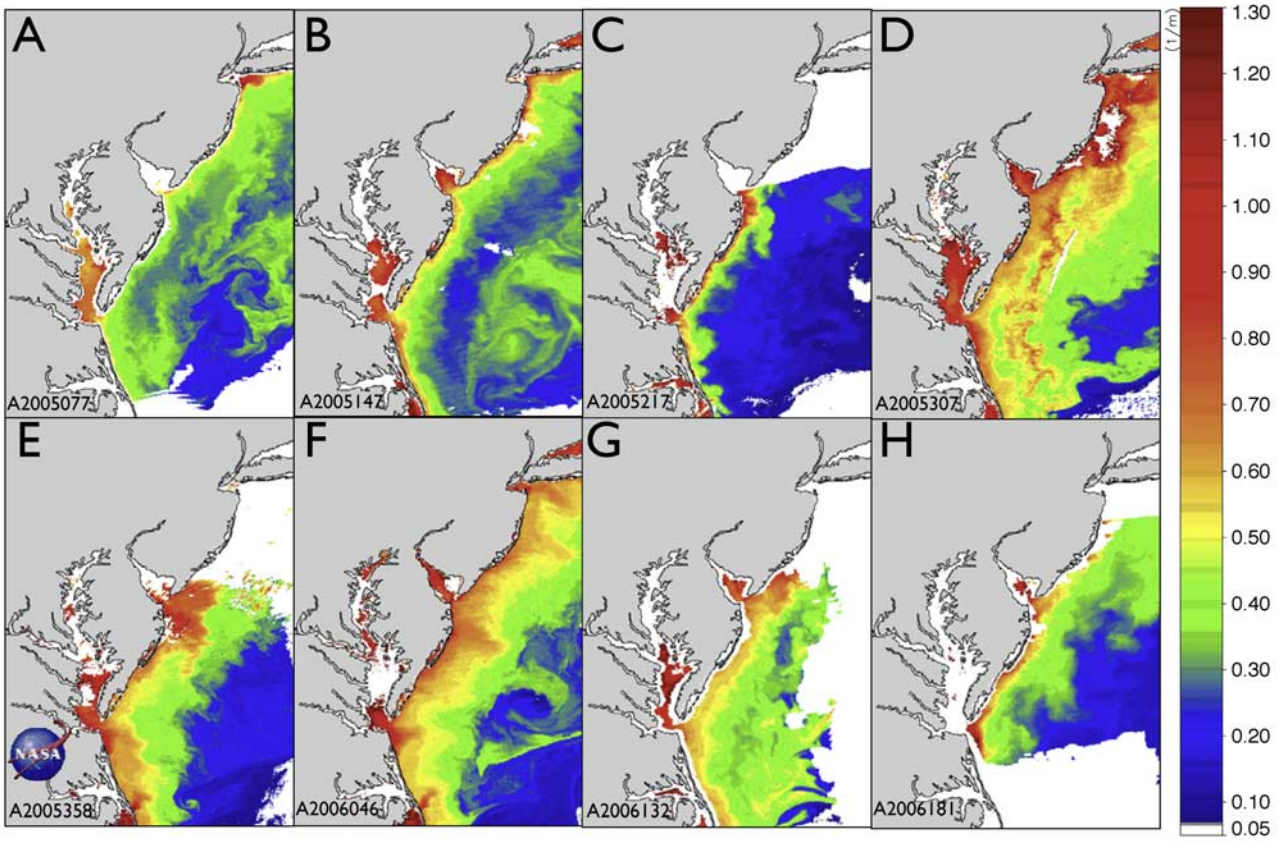

Figure 10. MODIS-Aqua derived satellite images of $a_{CDOM}(355)$ (m^{-1}) for (A) 18 March 2005, (B) 27 May 2005, (C) 5 August 2005, (D) 3 November 2005, (E) 24 December 2005, (F) 15 February 2006, (G) 12 May 2006, and (H) 30 June 2006. The CO_355M algorithm described in Table 1 was applied to derive the images shown.

3.3. Seasonal Variability of $a_{CDOM}(355)$ and DOC

[38] The satellite-derived products reveal strong seasonal variability in CDOM for the continental margin of the MAB. The gradient of high to low a_{CDOM} from the coast to the open ocean is consistent with our field measurements and previous work (Figure 10) [*Nelson and Guarda*, 1995; *DeGrandpre et al.*, 1996; *Del Vecchio and Blough*, 2004]. Higher levels of a_{CDOM} along the coast coincide with

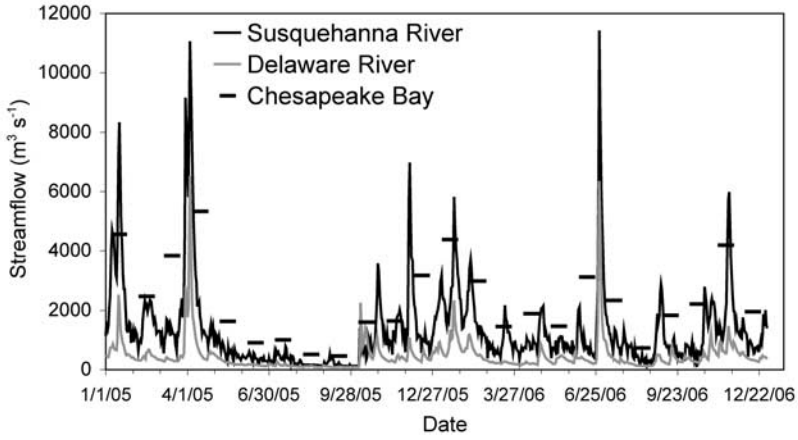

Figure 11. Daily streamflow from the Susquehanna River (Conowingo Dam, head of Chesapeake Bay) and Delaware River (Trenton, NJ) and monthly freshwater outflow from the Chesapeake Bay mouth. The Susquehanna River contributes >50% of the freshwater discharge into Chesapeake Bay. Data sources: http://waterdata.usgs.gov/nwis/; written communication from Gary Fisher, U.S. Geological Survey 17 July 2007.

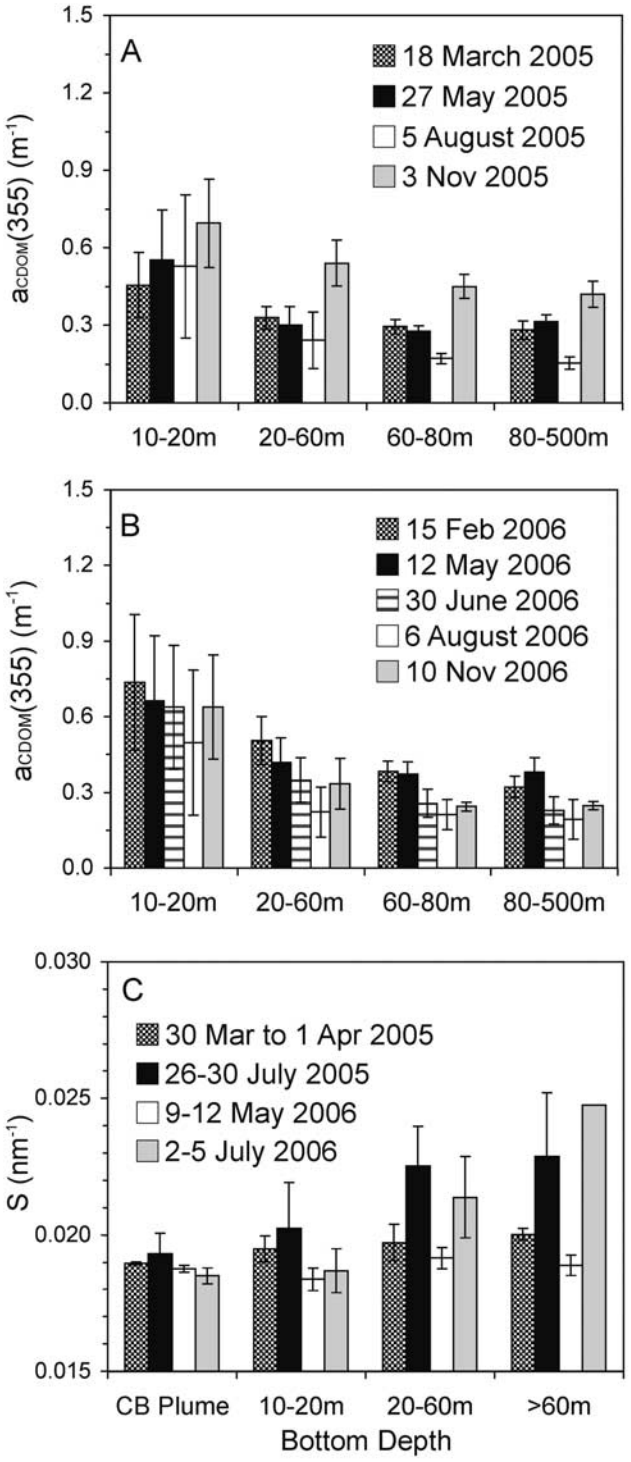

Figure 12. Seasonal variability of surface ocean a_{CDOM}(355) from discrete MODIS-Aqua images binned by bottom depth for (A) 2005, (B) 2006, and binned field measurements of the (C) CDOM spectral slope (S) for the Chesapeake Bay mouth and plume (CB Plume) and the continental shelf regions.

periods of elevated freshwater outflow from the Chesapeake Bay, Susquehanna River, and Delaware River, particularly during winter-spring (Figures 10–11; April to May 2005; November to December 2005 and February 2006). The offshore extent of the estuarine plumes is most pronounced in the a_{CDOM}(355) image from February 2006 (Figure 10F), which followed a period of several months with relatively high freshwater discharge (Figure 11). These results are consistent with several studies that have found seasonal and spatial variability in CDOM absorption with higher a_{CDOM} values in coastal waters during periods of high freshwater discharge [*Bricaud et al.*, 1981; *Nelson and Guarda*, 1995; *DeGrandpre et al.*, 1996; *Del Vecchio and Blough*, 2004].

[39] Satellite images of a_{CDOM}(355) suggest that both riverine/estuarine export (Figures 10 and 12) and upwelling along the shelf break (Figure 10D) contribute CDOM to the MAB. Degraded terrestrial vegetation transported by rivers and estuaries appears to be the principal source of CDOM to the continental margin [*Del Vecchio and Blough*, 2004]. Strong correlations between dissolved lignin phenols (compounds derived from vascular plants) and a_{CDOM}(350) were observed within the Mississippi River plume [*Hernes and Benner*, 2003] indicating a strong linkage between a_{CDOM} and terrestrial organic matter. Terrigenous DOM is characterized by strong absorption in the ultraviolet and blue wavelengths in part due to its high aromatic content from compounds such as lignin. These studies demonstrate that a_{CDOM} may be useful as a tracer of terrigenous DOM in the coastal ocean.

[40] Biological processes such as grazing and microbial activity may also contribute a_{CDOM} to the continental margin [*Nelson et al.*, 2004; *Steinberg et al.*, 2004]. *Chen et al.* [2002] observed significant inputs of fluorescent CDOM to the MAB from bottom water shelf-slope exchange and from upwelling of slope water in Georges Bank and concluded that rivers/estuaries contribute no more than 10% of CDOM fluorescence. During autumn, storm events vertically mix the water column and introduce CDOM-enriched bottom waters to the surface (Figure 10D). Seasonal vertical stratification isolates DOM at depth from sunlight, which can degrade CDOM, resulting in DOM with greater chromophoric content at depth than at the surface [*Vodacek et al.*, 1997; *Nelson and Siegel*, 2002]. Satellite-derived SST and a_{CDOM} can be applied to evaluate contributions of CDOM from the upwelling of CDOM-enriched bottom water derived from shelf-slope exchange, because upwelled waters are generally cooler than surrounding surface ocean waters.

[41] Substantial decreases in a_{CDOM}(355) were observed between spring and summer, particularly on the midshelf (20–60 m bottom depth), outer-shelf (60–80 m), and continental slope (80–500 m), presumably due to sunlight-induced photooxidation [*Vodacek et al.*, 1997, Figure 10, Figure 12]. Distributions of a_{CDOM}(355) from several discrete MODIS-Aqua images were binned by bottom depth across the study region (36°–39°N, 74°–77°W; region averaged is shown in Figure 13) using the 1 km SRTM30_Plus bathymetry data from *Becker and Sandwell* [2004] to estimate the seasonal change in CDOM (Figure 12). Between May to August, a_{CDOM}(355) decreased by 0.06 to 0.16 m^{-1} in 2005 and by 0.16 to 0.2 m^{-1} in 2006 from the midshelf to the continental slope region of the southern MAB (Figures 10 and 12). The increase in the CDOM spectral slope between spring and summer 2005 and 2006 also suggests that photooxidation significantly reduces CDOM in the southern MAB (Figure 12C).

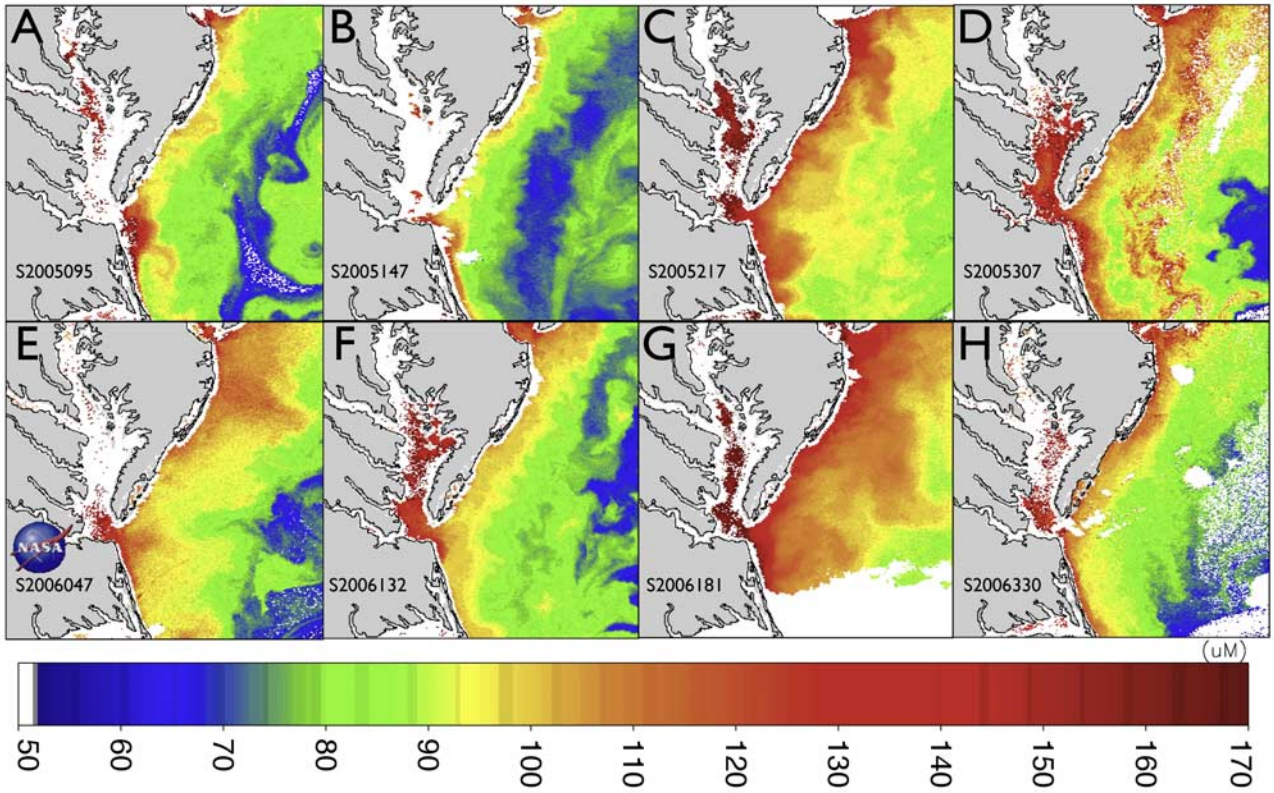

Figure 13. SeaWiFS derived satellite images of DOC (μmol C L^{-1}) for (A) 5 April 2005, (B) 27 May 2005, (C) 5 August 2005, (D) 3 November 2005, (E) 16 February 2006, (F) 12 May 2006, (G) 30 June 2006, and (H) 26 November 2006. The CO_DOC_{FWS} and CO_DOC_{Su} algorithms as described in Table 2 were applied to derive the images shown.

[42] The DOC distributions derived from satellite data analysis also reveal significant seasonal variability for the continental margin of the MAB (Figure 13). As observed for CDOM, DOC concentrations are generally higher along the coast, especially within the outflow regions of Chesapeake Bay and Delaware Bay, during and following periods of high freshwater discharge (April 2005, February 2006, June 2006, and November 2006; Figures 11 and 13) and decrease offshore. Much higher DOC concentrations are observed during the summer compared to early spring presumably due to net ecosystem production that promotes the accumulation of semilabile DOC (Figure 13). The seasonal accumulation of significant quantities of semilabile DOC typically begins near the end of phytoplankton blooms when nutrients become limiting, which promotes the excess production of organic carbon by phytoplankton [*Williams*, 1995; *Avril*, 2002; *Cauwet et al.*, 2002; *Nieto-Cid et al.*, 2004]. *Thingstad et al.* [1997] and *Fasham et al.* [1999] suggested that the spring to summer accumulation of DOC is related to microzooplankton predation on bacteria coupled with low bacterial growth rates, which would reduce DOC mineralization, during this period of low nutrient concentrations.

[43] DOC concentrations from several discrete MODIS-Aqua images were binned by bottom depth across the study region for comparison with field measurements and to estimate the seasonal NEP of DOC. The satellite-derived DOC values for 2005 and 2006 are in close agreement with the field measurements (Figure 14). Noteworthy differences ($\sim$13 μmol C L^{-1}) include the outer shelf and continental slope regions in 2006 (Figure 14B), which can be attributed, at least in part, to limited field sampling within those bathymetry regions. The seasonal increases in DOC concentration estimated from the discrete MODIS-Aqua images and field measurements are similar for 2005 and 2006 and range from 22–34 μmol C L^{-1} on the inner shelf (10–20 m), 18–31 μmol C L^{-1} on the midshelf (20–60 m), 13–19 μmol C L^{-1} on the outer shelf (60–80 m), and 12 μmol C L^{-1} on the continental slope (80–500 m) (Figure 14). The field measurements reveal a higher seasonal DOC increase on the midshelf (31 μmol C L^{-1}) and outer shelf (18.9 μmol C L^{-1}) for 2005 than observed from the MODIS images (18 and 13.3 μmol C L^{-1}, respectively), but similar values for 2006 (midshelf values of 23.6 and 21.4 μmol C L^{-1}, for field-based and MODIS-derived, respectively; outer shelf values of 15.5 and 16.1 μmol C L^{-1}, respectively) (Figure 14). The seasonal DOC increase computed in this study is consistent with previous field measurements collected by *Vlahos et al.* [2002] between March and August 1996 within the southern MAB (35 and 21 μmol C L^{-1} within the midshelf and continental slope region, respectively).

[44] From late autumn through early spring, the water column on the continental shelf is vertically well-mixed to at least 100 m, thus satellite retrievals of surface ocean products are representative of the entire water column. Field measurements of DOC and a_{CDOM} from March 2005 and May 2006 confirm this vertical homogeneity. Applying

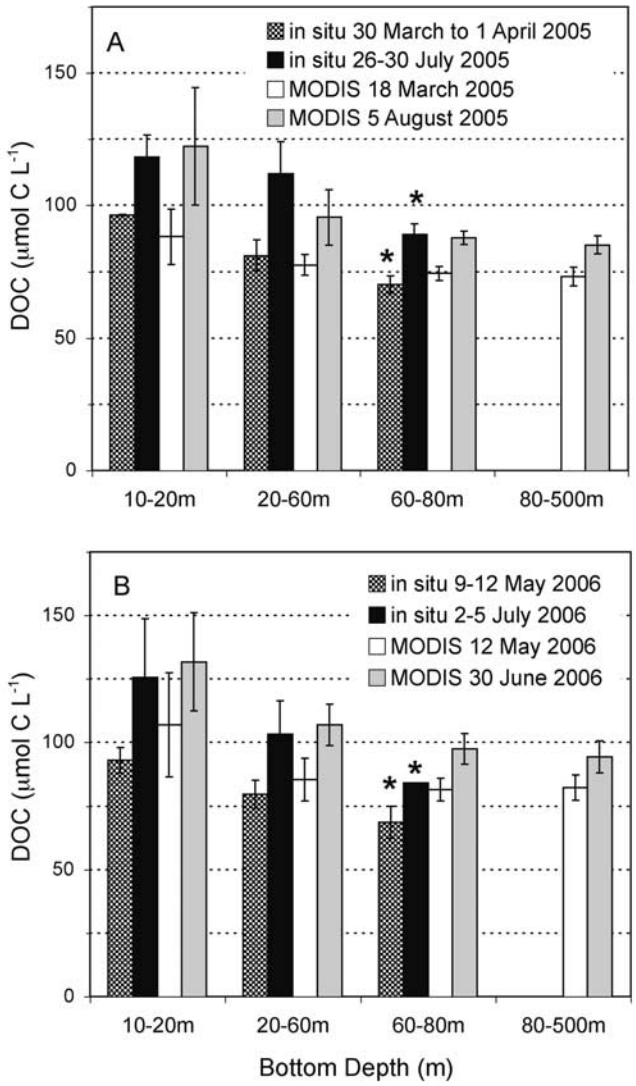

Figure 14. Seasonal increase of surface ocean DOC between spring and summer with comparisons of field measurements and discrete MODIS images binned by bottom depth from (A) 2005 and (B) 2006. The asterisk indicates that the field measurements shown were binned for stations >60 m.

MODIS-Aqua and SeaWiFS observations of surface ocean DOC and the high-resolution bathymetry data [*Becker and Sandwell*, 2004] yielded an estimate of the DOC reservoir of 1.1×10^{12} g C for the southern MAB (10–100 m bathymetry; 36° to 39°N; 77° to 74°W) during the winters of 2005 and 2006. Furthermore, by applying mixed-layer depths derived from climatological data and coupled physical-biogeochemical model results from the MAB [*Hofmann et al.*, 2008], the DOC reservoir and NEP of DOC can be estimated within the surface mixed-layer from satellite observations during stratified conditions.

4. Summary and Conclusions

[45] Validation analyses demonstrate successful retrieval of DOC and CDOM from coastal ocean waters using the MODIS-Aqua and SeaWiFS satellite sensors with an overall mean APD from field measurements of 9.3 ± 7.3% for DOC, 19 ± 14% for $a_{CDOM}(355)$, 15.5 ± 12% for $a_{CDOM}(443)$, and 8.6 ± 4.9% for the CDOM spectral slope. Clearly these algorithms meet the benchmark for a validated uncertainty of ±35% endorsed for the remote sensing retrieval of surface ocean chlorophyll a [*Bailey and Werdell*, 2006; *Hooker et al.*, 2007]. The results demonstrate slightly better retrievals of a_{CDOM} products with SeaWiFS than MODIS-Aqua, but equivalent retrievals for DOC and S.

[46] This study contributes the first validated algorithms for satellite retrieval of coastal ocean surface DOC, a_{CDOM}, and CDOM spectral slope. The a_{CDOM} satellite algorithms (e.g., CO_a355S and CO_a443M) can be applied beyond this study region, potentially to the global ocean. Appropriate field data sets are needed to extend the range of the exponential decay model (Figure 3A) for $a_{CDOM}(355)$ values less than 0.12 m^{-1} and greater than 1.3 m^{-1} and to validate these extended a_{CDOM} satellite products. The variability in the a_{CDOM} to DOC relationship limits the application of the specific DOC algorithm coefficients presented here to the continental shelf and slope area of the MAB (Table 2). Nevertheless, the approach presented here is valid for other coastal ocean regions where DOC is strongly correlated to a_{CDOM}. By adjusting the coefficients shown in Table 2 with values derived from other region-specific a_{CDOM} to DOC relationships [e.g., *Ferrari et al.*, 1996; *Del Castillo et al.*, 1999], regionally tuned CO_DOC_{FWS} (coastal ocean fall-winter-spring DOC) and CO_DOC_{Su} (coastal ocean summer DOC) algorithms may be applied "globally" within continental margins.

[47] The seasonal processes that influence CDOM distributions in the MAB include freshwater discharge (especially in winter and early spring), photooxidation in summer, and wind-induced vertical mixing of the water column in autumn. DOC distributions are driven primarily by freshwater discharge, net ecosystem production, and the ocean circulation pattern along the shelf and continental slope. The potential applications for satellite-derived CDOM and DOC products are substantial. Satellite analysis of a_{CDOM} can be used to quantify photooxidation rates (CDOM and DOC loss), track the inputs of terrigenous organic matter from rivers or estuaries into the coastal ocean and beyond, and trace water masses with different CDOM signatures. Satellite-derived DOC can be applied to carbon cycle studies to quantify the fluxes of DOC entering the coastal ocean and exported from the continental margin to the open ocean, estimate DOC produced through NEP, and assess the standing stock of DOC. With accurate satellite retrievals of surface ocean a_{CDOM} and DOC, satellite observations can be applied to investigate seasonal, interannual, and decadal-scale variability in CDOM and DOC within continental margins and evaluate how climate change and anthropogenic activities impact coastal ecosystems.

[48] **Acknowledgments.** This work has been supported by the NASA Ocean Biology and Biogeochemistry Program with grants from the NASA New Investigator Program, Interdisciplinary Science, and Earth Observing System programs and by NOAA through a grant in support of the Coastal Observatories program (NA03NOS4730220). We appreciate the constructive comments from the Associate Editor and two anonymous reviewers. We thank the Captains and crews of the R/V Cape Henlopen, R/V Hugh R. Sharp, and R/V Fay Slover. We are grateful to H. Throckmorton, P. Bernhardt, K. C. Filippino, C. Makinen, and M. Linksweiler for

help with particle filtration. Special thanks to J. Morrow, J. Brown, D. D'Alimonte, and J.-N. Druon for assistance with deploying the profiling radiometer, L. Van Heukelem and C. Thomas (Horn Point Laboratory) for the HPLC pigment results, S. Bailey and J. Werdell for reviewing an earlier draft of this manuscript, and the Ocean Biology Processing Group (OBPG) at GSFC. J. O'Reilly kindly provided the high-resolution bathymetry data. Field measurements presented in this article were submitted to the NASA SeaWiFS Bio-optical Archive and Storage System (SeaBASS).

References

Aiken, J., G. F. Moore, and P. M. Holligan (1992), Remote sensing of oceanic biology in relation to global climate change, *J. Phycol.*, *28*, 549–590.

Álvarez-Salgado, X. A., J. Gago, B. M. Míguez, and F. F. Pérez (2001), Net ecosystem production of dissolved organic carbon in a coastal upwelling system: The Ría de Vigo, Iberian margin of the North Atlantic, *Limnol. Oceanogr.*, *46*, 135–147.

Avril, B. (2002), DOC dynamics in the northwestern Mediterranean Sea (DYFAMED site), *Deep Sea Res.*, *49*, 2163–2182.

Bailey, S. W., and P. J. Werdell (2006), A multi-sensor approach for the on-orbit validation of ocean color satellite data products, *Remote Sens. Environ.*, *102*, 12–23.

Bailey, S. W., W. D. Robinson, and B. A. Franz (2003), Modifications to SeaWiFS NIR correction, in *Algorithm Updates for the Fourth SeaWiFS Data Reprocessing*, *NASA Technical Memo. 2003-206892*, vol. 22, edited by S. B. Hooker and E. R. Firestone, pp. 26–28, NASA Goddard Space Flight Cent., Greenbelt, Md.

Bates, N. R., and D. A. Hansell (1999), A high resolution study of surface layer hydrographic and biogeochemical properties between Chesapeake Bay and Bermuda, *Mar. Chem.*, *67*, 1–16.

Becker, J. J., and D. T. Sandwell (2004), *SRTM30_PLUS: Data Fusion of SRTM Land Topography With Measured and Estimated Seafloor Topography*, Scripps Inst. Oceanogr., Univ. Calif. San Diego, La Jolla, Calif.

Benner, R., and M. Strom (1993), A critical evaluation of the analytical blank associated with DOC measurements by high-temperature catalytic oxidation, *Mar. Chem.*, *41*, 153–160.

Blough, N. V., and R. Del Vecchio (2002), Chromophoric DOM in the coastal environment, in *Biogeochemistry of Marine Dissolved Organic Matter*, edited by D. A. Hansell and C. A. Carlson, pp. 509–546, Academic Press, San Diego, Calif.

Bricaud, A., A. Morel, and L. Prieur (1981), Absorption by dissolved organic matter of the sea (yellow substance) in the UV and visible domains, *Limnol. Oceanogr.*, *26*, 43–53.

Carder, K. L., R. G. Steward, G. R. Harvey, and P. B. Ortner (1989), Marine humic and fulvic acids: Their effects on remote sensing of ocean chlorophyll, *Limnol. Oceanogr.*, *34*, 68–81.

Carder, K. L., F. R. Chen, Z. P. Lee, S. K. Hawes, and D. Kamykowski (1999), Semianalytic Moderate-Resolution Imaging Spectrometer algorithms for chlorophyll and absorption with bio-optical domains based on nitrate-depletion temperatures, *J. Geophys. Res.*, *104*(C3), 5403–5421.

Cauwet, G., G. Déliat, A. Krastev, G. Shtereva, S. Becquevort, C. Lancelot, A. Momzikoff, A. Saliot, A. Cociasu, and L. Popa (2002), Seasonal DOC accumulation in the Black Sea: A regional explanation for a general mechanism, *Mar. Chem.*, *79*, 193–205.

Chen, R. F., Y. Zhang, P. Vlahos, and S. M. Rudnick (2002), The fluorescence of dissolved organic matter in the Mid-Atlantic Bight, *Deep Sea Res., Part II*, *49*, 4439–4459.

Churchill, J. H., and T. J. Berger (1998), Transport of Middle Atlantic Bight shelf water to the Gulf Stream near Cape Hatteras, *J. Geophys. Res.*, *103*(C13), 30,605–30,621.

Claustre, H., et al. (2004), An intercomparison of HPLC phytoplankton pigment methods using in situ samples: Application to remote sensing and database activities, *Mar. Chem.*, *85*, 41–61.

DeGrandpre, M. D., A. Vodacek, R. K. Nelson, E. J. Bruce, and N. V. Blough (1996), Seasonal seawater optical properties of the U.S. Middle Atlantic Bight, *J. Geophys. Res.*, *101*(C10), 22,727–22,736.

Del Castillo, C. E., P. G. Coble, J. M. Morell, J. M. Lopez, and J. E. Corredor (1999), Analysis of the optical properties of the Orinoco River plume by absorption and fluorescence spectroscopy, *Mar. Chem.*, *66*, 35–51.

Del Vecchio, R., and N. V. Blough (2004), Spatial and seasonal distribution of chromophoric dissolved organic matter (CDOM) and dissolved organic carbon (DOC) in the Middle Atlantic Bight, *Mar. Chem.*, *89*, 169–187.

Del Vecchio, R., and A. Subramaniam (2004), Influence of the Amazon River on the surface optical properties of the western tropical North Atlantic Ocean, *J. Geophys. Res.*, *109*, C11001, doi:10.1029/2004JC002503.

D'Sa, E. J., and R. L. Miller (2003), Bio-optical properties in waters influenced by the Mississippi River during low flow conditions, *Remote Sens. Environ.*, *84*, 538–549.

Fasham, M. J. R., P. W. Boyd, and G. Savidge (1999), Modeling the relative contributions of autotrophs and heterotrophs to carbon flow at a Lagrangian JGOFS station in the Northeast Atlantic: The importance of DOC, *Limnol. Oceanogr.*, *44*, 80–94.

Ferrari, G. M., M. D. Dowell, S. Grossi, and C. Targa (1996), Relationship between the optical properties of chromophoric dissolved organic matter and total concentrations of dissolved organic carbon in the southern Baltic Sea region, *Mar. Chem.*, *55*, 299–316.

Garcia, V. M. T., S. Signorini, C. A. E. Garcia, and C. R. McClain (2006), Empirical and semi-analytical chlorophyll algorithms in the south-western Atlantic coastal region (25–40°S and 60–45°W), *Int. J. Remote Sens.*, *27*, 1539–1562.

Hansell, D. A., and C. A. Carlson (1998), Net community production of dissolved organic carbon, *Global Biogeochem. Cycles*, *12*(3), 443–453.

Hedges, J. I. (2002), Why dissolved organic matter, in *Biogeochemistry of Marine Dissolved Organic Matter*, edited by D. A. Hansell and C. A. Carlson, pp. 1–33, Academic Press, San Diego, Calif.

Hernes, P. J., and R. Benner (2003), Photochemical and microbial degradation of dissolved lignin phenols: Implications for the fate of terrigenous dissolved organic matter in marine environments, *J. Geophys. Res.*, *108*(C9), 3291, doi:10.1029/2002JC001421.

Hofmann, E., et al. (2008), Eastern U.S. Continental Shelf carbon budget: Integrating models, data assimilation, and analysis, *Oceanography*, *21*, 86–104.

Hoge, F. E., C. W. Wright, P. E. Lyon, R. N. Swift, and J. K. Yungel (2001), Inherent optical properties imagery of the western North Atlantic Ocean: Horizontal spatial variability of the upper mixed layer, *J. Geophys. Res.*, *106*(C12), 31,129–31,138.

Hooker, S. B., and J. Aiken (1998), Calibration evaluation and radiometric testing of field radiometers with the SeaWiFS Quality Monitor (SQM), *J. Atmos. Oceanic Technol.*, *15*, 995–1007.

Hooker, S. B., and S. Maritorena (2000), An evaluation of oceanographic radiometers and deployment methodologies, *J. Atmos. Oceanic Technol.*, *17*, 811–830.

Hooker, S. B., and C. R. McClain (2000), The calibration and validation of SeaWiFS data, *Prog. Oceanogr.*, *45*, 427–465.

Hooker, S. B., and A. Morel (2003), Platform and environmental effects on above- and in-water determinations of water-leaving radiances, *J. Atmos. Oceanic Technol.*, *20*, 187–205.

Hooker, S. B., and G. Zibordi (2005), Advanced methods for characterizing the immersion factor of irradiance sensors, *J. Atmos. Oceanic Technol.*, *22*, 757–770.

Hooker, S. B., G. Zibordi, J.-F. Berthon, D. D'Alimonte, S. Maritorena, S. McLean, and J. Sildam (2001), *Results of the Second SeaWiFS Data Analysis Round Robin, March 2000 (DARR-00)*, *NASA Tech. Memo. 2001-206892*, vol. 15, edited by S. B. Hooker and E. R. Firestone, 71 pp., NASA Goddard Space Flight Cent., Greenbelt, Md.

Hooker, S. B., S. McLean, J. Sherman, M. Small, G. Lazin, G. Zibordi, and J. W. Brown (2002a), *The Seventh SeaWiFS Intercalibration Round-Robin Experiment (SIRREX-7), March 1999*, *NASA Tech. Memo, 2002-206892*, vol. 17, edited by S. B. Hooker and E. R. Firestone, 69 pp., NASA Goddard Space Flight Cent., Greenbelt, Md.

Hooker, S. B., G. Lazin, G. Zibordi, and S. McLean (2002b), An evaluation of above- and in-water methods for determining water-leaving radiances, *J. Atmos. Oceanic Technol.*, *19*, 486–515.

Hooker, S. B., et al. (2005), *The Second SeaWiFS HPLC Analysis Round-Robin Experiment (SeaHARRE-2)*, *NASA Tech. Memo. 2005-212785*, 112 pp., NASA Goddard Space Flight Cent., Greenbelt, Md.

Hooker, S. B., C. R. McClain, and A. Mannino (2007), *NASA Strategic Planning Document: A Comprehensive Plan for the Long-Term Calibration and Validation of Oceanic Biogeochemical Satellite Data*, *NASA Special Pub. 2007-214152*, 31 pp., NASA Goddard Space Flight Cen., Greenbelt, Md.

Jahnke, R. A. (2008), Global synthesis, in *Carbon and Nutrient Fluxes in Continental Margins: A Global Synthesis*, edited by K. K. Liu et al., Global Change: The IGBP Series, Springer-Verlag, New York, in press.

Johannessen, S. C., W. L. Miller, and J. J. Cullen (2003), Calculation of UV attenuation and colored dissolved organic mater absorption spectra from measurements of ocean color, *J. Geophys. Res.*, *108*(C9), 3301, doi:10.1029/2000JC000514.

Kahru, M., and B. G. Mitchell (2001), Seasonal and nonseasonal variability of satellite-derived chlorophyll and colored dissolved organic matter concentration in the California current, *J. Geophys. Res.*, *106*(C2), 2517–2529.

Lebo, M. E., and J. H. Sharp (1993), Phosphorus distributions along the Delaware: An urbanized coastal plain estuary, *Estuaries*, *16*, 291–302.

Lee, Z. P., K. L. Carder, and R. A. Arnone (2002), Deriving inherent optical properties from water color: A multiband quasi-analytical algorithm for optically deep waters, *Appl. Opt.*, *41*, 5755–5772.

Ludwig, W., J.-L. Probst, and S. Kempe (1996), Predicting the oceanic input of organic carbon by continental erosion, *Global Biogeochem. Cycles*, *10*(1), 23–41.

Magnuson, A., L. W. Harding Jr., M. E. Mallonee, and J. E. Adolf (2004), Bio-optical model for Chesapeake Bay and Middle Atlantic Bight, *Estuarine Coastal Shelf Sci.*, *61*, 403–424.

Mannino, A., and H. R. Harvey (1999), Lipid composition in particulate and dissolved organic matter in the Delaware Estuary: Sources and diagenetic patterns, *Geochim. Cosmochim. Acta*, *63*, 2219–2235.

Mannino, A., and H. R. Harvey (2000), Terrigenous dissolved organic matter along an estuarine gradient and its flux to the coastal ocean, *Org. Geochem.*, *31*, 1611–1625.

Mannino, A., and H. R. Harvey (2004), Black carbon in estuarine and coastal ocean dissolved organic matter, *Limnol. Oceanogr.*, *49*, 735–740.

Mantoura, R. F. C., and E. M. S. Woodward (1983), Conservative behavior of riverine dissolved organic carbon in the Severn estuary: Chemical and geochemical implications, *Geochim. Cosmochim. Acta*, *47*, 1293–1309.

Maritorena, S., D. A. Siegel, and A. R. Peterson (2002), Optimization of a semianalytical ocean color model for global-scale applications, *Appl. Opt.*, *41*, 2705–2714.

McKee, B. A. (2003), RiOMar: The Transport, Transformation and Fate of Carbon in River-dominated Ocean Margins, Report of the RiOMar Workshop, 1–3 November 2001, Tulane Univ., New Orleans, La.

Mitchell, B. G., et al. (2000), Determination of spectral absorption coefficients of particles, dissolved material and phytoplankton for discrete water samples, in *Ocean Optics Protocols for Satellite Ocean Color Sensor Validation*, edited by G. S. Fargion and J. L. Mueller, pp. 125–153, NASA/TM-2000-209966, NASA Goddard Space Flight Cent., Greenbelt, MD.

Mitchell, B. G., M. Kahru, J. Wieland, and M. Stramska (2003), Determination of spectral absorption coefficients of particles, dissolved material and phytoplankton for discrete water samples, in *Ocean Optics Protocols for Satellite Ocean Color Sensor Validation*, edited by G. S. Fargion, J. L. Mueller, and C. R. McClain, pp. 39–64, NASA/TM-2003-211621/Rev4-Vol.IV, NASA Goddard Space Flight Cent., Greenbelt, MD.

Mueller, J. L. (2003), Overview of measurement and data analysis methods, in *Ocean Optics Protocols for Satellite Ocean Color Sensor Validation, Revision 4, Volume III: Radiometric Measurements and Data Analysis Protocols*, edited by J. L. Mueller et al., NASA Tech. Memo. 2003-211621/Rev4-vol. III, pp. 1–20, NASA Goddard Space Flight Cent., Greenbelt, Md.

Nelson, J. R., and S. Guarda (1995), Particulate and dissolved spectral absorption on the continental shelf of the southeastern United States, *J. Geophys. Res.*, *100*, 8715–8732.

Nelson, N. B., and D. A. Siegel (2002), Chromophoric DOM in the open ocean, in *Biogeochemistry of Marine Dissolved Organic Matter*, edited by D. A. Hansell and C. A. Carlson, pp. 547–578, Academic Press, San Diego, Calif.

Nelson, N. B., C. A. Carlson, and D. K. Steinberg (2004), Production of chromophoric dissolved organic matter by Sargasso Sea microbes, *Mar. Chem.*, *89*, 273–287.

Nieto-Cid, M., X. A. Álvarez-Salgado, S. Brea, and F. F. Perez (2004), Cycling of dissolved and particulate carbohydrates in a coastal upwelling system (NW Iberian Peninsula), *Mar. Ecol. Prog. Ser.*, *283*, 39–54.

O'Reilly, J. E., S. Maritorena, B. G. Mitchell, D. A. Siegel, K. L. Carder, S. A. Garver, M. Kahru, and C. R. McClain (1998), Ocean color chlorophyll algorithms for SeaWiFS, *J. Geophys. Res.*, *103*(C11), 24,937–24,953.

O'Reilly, J. E., et al. (2000), Ocean color chorophyll a Algorithms for SeaWiFS, OC2, and OC4: Version 4, in *SeaWiFS Postlaunch Calibration and Validation Analyses, Part 3*, edited by S. B. Hooker and E. R. Firestone, NASA Tech. Memo. 2000-206892, vol. 11, pp. 9–23, NASA Goddard Space Flight Cent., Greenbelt, Md.

Rennie, S. E., J. J. Largier, and S. J. Lentz (1999), Observations of a pulsed buoyancy current downstream of Chesapeake Bay, *J. Geophys. Res.*, *104*(C8), 18,227–18,240.

Rochelle-Newall, E. J., and T. R. Fisher (2002), Chromophoric dissolved organic matter and dissolved organic carbon in Chesapeake Bay, *Mar. Chem.*, *77*, 23–41.

Sanders, T. M., and R. W. Garvine (2001), Fresh water delivery to the continental shelf and subsequent mixing: An observational study, *J. Geophys. Res.*, *106*(C11), 27,087–27,101.

Schlünz, B., and R. R. Schneider (2000), Transport of terrestrial organic carbon to the oceans by rivers: Re-estimating flux- and burial rates, *Int. J. Earth Sci.*, *88*, 599–606.

Schubel, J. R., and D. W. Pritchard (1986), Responses of upper Chesapeake Bay to variations in discharge of the Susquehanna River, *Estuaries*, *9*, 236–249.

Sharp, J. H., C. A. Carlson, E. T. Peltzer, D. M. Castle-Ward, K. B. Savidge, and K. R. Rinker (2002), Final dissolved organic carbon broad community intercalibration and preliminary use of DOC reference materials, *Mar. Chem.*, *77*, 239–253.

Siegel, D. A., M. Wang, S. Maritorena, and W. D. Robinson (2000), Atmospheric correction of satellite ocean-color imagery: The black pixel assumption, *Appl. Opt.*, *39*, 3582–3591.

Siegel, D. A., S. Maritorena, N. B. Nelson, D. A. Hansell, and M. Lorenzi-Kayser (2002), Global distribution and dynamics of colored dissolved and detrital organic materials, *J. Geophys. Res.*, *107*(C12), 3228, doi:10.1029/2001JC000965.

Siegel, D. A., S. Maritorena, N. B. Nelson, and M. J. Behrenfeld (2005), Independence and interdependencies among global ocean color properties: Reassessing the bio-optical assumption, *J. Geophys. Res.*, *110*, C07011, doi:10.1029/2004JC002527.

Smith, R. C., and K. S. Baker (1984), Analysis of ocean optical data, in *Ocean Optics VII*, edited by M. A. Blizard, *Proc. SPIE Int. Soc. Opt. Eng.*, vol. 489, pp. 119–126, Bellingham, WA.

Steinberg, D. K., N. Nelson, C. A. Carlson, and A. C. Prusak (2004), Production of chromophoric dissolved organic matter (CDOM) in the open ocean by zooplankton and the colonial cyanobacterium Trichodesmium spp., *Mar. Ecol. Prog. Ser.*, *267*, 45–56.

Thingstad, T. F., Å. Hagström, and F. Rassoulzadegan (1997), Accumulation of degradable DOC in surface waters: Is it caused by a malfunctioning microbial loop?, *Limnol. Oceanogr.*, *42*, 398–404.

Van Heukelem, L., and C. S. Thomas (2001), Computer-assisted high-performance liquid chromatography method development with applications to the isolation and analysis of phytoplankton pigments, *J. Chromatogr. A*, *910*, 31–49.

Verity, P. G., J. E. Bauer, C. N. Flagg, D. J. DeMaster, and D. J. Repeta (2002), The Ocean Margins Program: An interdisciplinary study of carbon sources, transformations, and sinks in a temperate continental margin system, *Deep Sea Res., Part II*, *49*, 4273–4295.

Vlahos, P., R. F. Chen, and D. J. Repeta (2002), Dissolved organic carbon in the Middle Atlantic Bight, *Deep Sea Res., Part II*, *49*, 4369–4385.

Vodacek, A., F. E. Hoge, R. N. Swift, J. K. Yungel, E. T. Peltzer, and N. V. Blough (1995), The use of in situ and airborne fluorescence measurements to determine UV absorption coefficients and DOC concentrations in surface waters, *Limnol. Oceanogr.*, *40*, 411–415.

Vodacek, A., N. V. Blough, M. D. DeGrandpre, E. T. Peltzer, and R. K. Nelson (1997), Seasonal variation of CDOM and DOC in the Middle Atlantic Bight: Terrestrial inputs and photooxidation, *Limnol. Oceanogr.*, *42*, 674–686.

Wang, M., and W. Shi (2005), Estimation of ocean contribution at the MODIS near-infrared wavelengths along the east coast of the U.S.: Two case studies, *Geophys. Res. Lett.*, *32*, L13606, doi:10.1029/2005GL022917.

Williams, P. J. leB. (1995), Evidence for the seasonal accumulation of carbon-rich dissolved organic material, its scale in comparison with changes in particulate material and the consequential effect on net C/N assimilation ratios, *Mar. Chem.*, *51*, 17–29.

Yuan, J., M. J. Dagg, and C. E. Del Castillo (2005), In-pixel variations of chl a fluorescence in the Northern Gulf of Mexico and their implications for calibrating remotely sensed chl a and other products, *Cont. Shelf Res.*, *25*, 894–904.

S. B. Hooker, A. Mannino, and M. E. Russ, Hydrospheric and Biospheric Sciences Laboratory, NASA Goddard Space Flight Center, Mail Code 614.2, Greenbelt, MD 20771, USA. (antonio.mannino@nasa.gov)